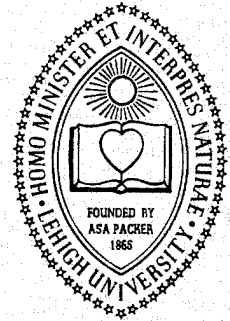


LEHIGH UNIVERSITY



NORMAL AND RADIAL IMPACT OF COMPOSITES WITH EMBEDDED PENNY-SHAPED CRACKS

BY

G. C. SIH AND E. P. CHEN

FEBRUARY 1979

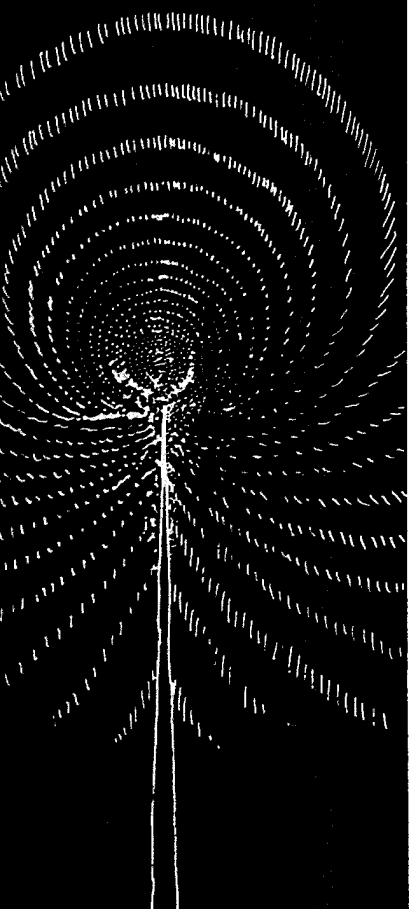
MATERIALS AND STRUCTURES DIVISION
NASA-LEWIS RESEARCH CENTER
CLEVELAND, OHIO 44135

DISTRIBUTION STATEMENT A

Approved for public release;
Distribution Unlimited

DTIC QUALITY INSPECTED 1

TO ETC-1-102-
O-106 D2A MDC-10ADP
NO-2AICMS



19960229 111

PLASTIC 33184

1. Report No. NASA CR 159538	2. Government Accession No.	3. Recipient's Catalog No.	
4. Title and Subtitle NORMAL AND RADIAL IMPACT OF COMPOSITES WITH EMBEDDED PENNY-SHAPED CRACKS		5. Report Date February 1979	
		6. Performing Organization Code	
7. Author(s) Dr. G. C. Sih and Dr. E. P. Chen		8. Performing Organization Report No.	
		10. Work Unit No.	
9. Performing Organization Name and Address Lehigh University Institute of Fracture and Solid Mechanics Bethlehem, PA 18015		11. Contract or Grant No. NSG 3179	
		13. Type of Report and Period Covered Interim Report	
12. Sponsoring Agency Name and Address National Aeronautics and Space Administration Washington DC 20546		14. Sponsoring Agency Code	
		15. Supplementary Notes Project Manager: Christos C. Chamis Materials and Structures Division NASA-Lewis Research Center 21000 Brookpark Road, M.S. 49-3 Cleveland, OH 44135	
16. Abstract A method is developed for the dynamic stress analysis of a layered composite containing an embedded penny-shaped crack and subjected to normal and radial impact. The material properties of the layers are chosen such that the crack lies in a layer of matrix material while the surrounding material possesses the average elastic properties of a two-phase medium consisting of a large number of fibers embedded in the matrix. Quantitatively, the time-dependent stresses near the crack border can be described by the dynamic stress intensity factors. Their magnitude depends on time, on the material properties of the composite and on the relative size of the crack compared to the composite local geometry. Results obtained show that, for the same material properties and geometry of the composite, the dynamic stress intensity factors for an embedded (penny-shaped) crack reach their peak values within a shorter period of time and with a lower magnitude than the corresponding dynamic stress intensity factors for a through-crack.			
17. Key Words (Suggested by Author(s)) Composites, normal impact, radial impact, penny-shaped crack, elastodynamics, stress analysis, stress intensity, Laplace transform, Fourier transform, Fredholm integral equations.		18. Distribution Statement Unclassified	
19. Security Classif. (of this report) Unclassified	20. Security Classif. (of this page) Unclassified	21. No. of Pages 33	22. Price*

* For sale by the National Technical Information Service, Springfield, Virginia 22161

FOREWORD

This research work deals with the normal and radial impact of composites with embedded penny-shaped cracks which represents a portion of the program supported by the NASA-Lewis Research Center in Cleveland, Ohio. The program covers the period from February 13, 1978 to February 12, 1979 under Grant NSG 3179 and is conducted by the Institute of Fracture and Solid Mechanics at Lehigh University.

Professor George C. Sih served as the Principal Investigator while Dr. E. P. Chen was the Associate Investigator who is now employed by the Sandia Laboratory in New Mexico. The capable guidance of Dr. Christos C. Chamis who acted as the NASA Project Manager is very much appreciated. His encouragement has led to the success of this work.

TABLE OF CONTENTS

FOREWORD	iv
TABLE OF CONTENTS	v
LIST OF FIGURES	vi
LIST OF SYMBOLS	
ABSTRACT	1
INTRODUCTION	2
AXIAL SYMMETRIC DEFORMATION: PENNY-SHAPED CRACK	3
NORMAL IMPACT	7
<i>Fredholm integral equations</i>	8
<i>Stress intensity factor for normal impact</i>	9
RADIAL IMPACT	11
<i>Integral equations</i>	12
<i>Stress intensity factor for radial impact</i>	14
CONCLUDING REMARKS	15
APPENDIX: EXPRESSIONS FOR $A^{(i)}(s,p), \dots, C^{(i)}(s,p)$	16
<i>Radial impact</i>	18
ACKNOWLEDGEMENTS	19
REFERENCES	19
FIGURES	21
COMPUTER PROGRAMS	
<i>Axial impact</i>	34
<i>Torsional impact</i>	41

LIST OF FIGURES

Figure 1	- Penny-shaped crack embedded in a matrix layer under normal and radial impact	21
Figure 2	- Plot of $\Lambda_I^*(1,p)$ versus c_{21}/pa for $a/b = 1.0$	22
Figure 3	- Plot of $\Lambda_I^*(1,p)$ versus c_{21}/pa for $\mu_2/\mu_1 = 0.1$	23
Figure 4	- Plot of $\Lambda_I^*(1,p)$ versus c_{21}/pa for $\mu_2/\mu_1 = 10.0$	24
Figure 5	- Dynamic stress intensity factor $k_1(t)$ for penny-shaped crack with $a/b = 1.0$	25
Figure 6	- Dynamic stress intensity factor $k_1(t)$ for penny-shaped crack with $\mu_2/\mu_1 = 0.1$	26
Figure 7	- Dynamic stress intensity factor $k_1(t)$ for penny-shaped crack with $\mu_2/\mu_1 = 10.0$	27
Figure 8	- Variations of $\Lambda_{II}^*(1,p)$ with c_{21}/pa for $a/b = 1.0$	28
Figure 9	- Variations of $\Lambda_{II}^*(1,p)$ with c_{21}/pa for $\mu_2/\mu_1 = 0.1$ and varying a/b	29
Figure 10	- Variations of $\Lambda_{II}^*(1,p)$ with c_{21}/pa for $\mu_2/\mu_1 = 10$ and varying a/b	30
Figure 11	- Stress intensity factor $k_2(t)$ versus time for a penny-shaped crack with $a/b = 1.0$	31
Figure 12	- Stress intensity factor $k_2(t)$ versus time for a penny-shaped crack with $\mu_2/\mu_1 = 0.1$	32
Figure 13	- Stress intensity factor $k_2(t)$ versus time for a penny-shaped crack with $\mu_2/\mu_1 = 10.0$	33

LIST OF SYMBOLS

a	- radius of crack
$A(s,p), B(s,p)$	- unknowns in dual integral equations
$A^{(i)}, B^{(i)}, C^{(i)}$	- coefficients for transform of solution, functions of (s,p)
b	- half of the thickness of the layer
Br	- Bromwich contour in the complex p -plane
c_{1j}, c_{2j}	- dilatational and shear wave speeds for medium j
$e^{(i)}$	- functions of (p,s) through γ_{ij}
$f^*(p)$	- Laplace transform of $f(t)$
$f^h(s)$	- Hankel transform of $f(x)$
$(f)_j$	- indicates that f is evaluated in medium j
$h(t)$	- Heaviside unit step function
$J_n(x)$	- Bessel function of order n
$k_1(t), k_2(t)$	- dynamic stress intensity factors
$M_I(\xi, n, p)$	- kernel of Fredholm integral equation
$M_{II}(\xi, n, p)$	- kernel in dual integral equations
$P_I(s,p), P_{II}(s,p)$	- kernel in dual integral equations
r, θ, z	- cylindrical coordinates
r_1, θ_1	- crack tip polar coordinates
u_r, u_θ	- displacement components
t	- time
x, y, z	- rectangular coordinates - crack lies in the xy -plane
γ_{ij}	- exponents for transform of solution, functions of (p,s)
$\delta^{(i)}$	- functions of (p,s) through $e^{(i)}$
Δ_I, Δ_{II}	- functions of (p,s) through $\delta^{(i)}$
λ_1, λ_2	- Lamé coefficient

$\Lambda_I^*(\xi, p), \Lambda_{II}^*(\xi, p)$ - unknown in Fredholm integral equation
 μ_1, μ_2 - shear modulus
 ν_1, ν_2 - Poisson's ratio
 ρ_1, ρ_2 - mass density
 σ_0 - suddenly applied normal stress
 $\sigma_r, \sigma_\theta, \sigma_z, \tau_{rz}$ - stress components
 τ_0 - suddenly applied shear stress
 ϕ_j, ψ_j - scalar potentials for medium j
 ∇^2 - Laplacian operator

NORMAL AND RADIAL IMPACT OF COMPOSITES
WITH EMBEDDED PENNY-SHAPED CRACKS

by

G. C. Sih
Institute of Fracture and Solid Mechanics
Lehigh University
Bethlehem, Pennsylvania 18015

and

E. P. Chen^{*}
Sandia Laboratories
Albuquerque, New Mexico 87115

ABSTRACT

A method is developed for the dynamic stress analysis of a layered composite containing an embedded penny-shaped crack and subjected to normal and radial impact. The material properties of the layers are chosen such that the crack lies in a layer of matrix material while the surrounding material possesses the average elastic properties of a two-phase medium consisting of a large number of fibers embedded in the matrix. Quantitatively, the time-dependent stresses near the crack border can be described by the dynamic stress intensity factors. Their magnitude depends on time, on the material properties of the composite and on the relative size of the crack compared to the composite local geometry. Results obtained show that, for the same material properties and geometry of the composite, the dynamic stress intensity factors for an embedded (penny-shaped) crack reach their peak values within a shorter period of time and with a lower magnitude than the corresponding dynamic stress factors for a through-crack.

*This work was completed when Dr. Chen was a faculty member at Lehigh University.

INTRODUCTION

Advanced composite materials are multi-phased nonhomogeneous materials with anisotropic properties. This complicates the stress analysis for fracture, particularly if the loading is time-dependent and the geometry involves sharp edges such as a crack. As a result, conventional and mathematical techniques for dynamic fracture generally fail to yield accurate results.

An effective approach for finding dynamic stresses in a nonhomogeneous composite containing a through crack has been developed [1] by utilizing both the Laplace and Fourier transforms. The transient boundary, symmetry and continuity conditions were formulated by integral representations in terms of the rectangular Cartesian coordinates x and y and the results for the stress intensity factors are determined numerically by solving a standard integral equation in the Laplace transform plane. The crack geometry was assumed to be extended infinitely in the z -direction or through the side wall of the composite specimen. Many of the failures in composites, however, were observed [2] to initiate from embedded mechanical imperfections such as air bubbles, voids or cavities. Hence, a more realistic modeling of the actual flaw geometry would be an embedded crack that has finite dimensions in all directions. This immediately suggests a three-dimensional elastodynamic crack problem which cannot be solved effectively by analytical means unless symmetry prevails. One approach for obtaining a solution is to extend the integral transform formulation for a through crack in rectangular coordinates [1] to that of an embedded crack in cylindrical polar coordinates. This necessitates the use of Hankel transforms instead of Fourier transforms.

Although no attempt will be made to analyze the failure of the composite due to impact, the dynamic stress intensity factors $k_1(t)$ and $k_2(t)$ can be readily

used in a given fracture criterion, say the strain energy density theory [3], for determining the allowable level of impact load. The new results can also assist the construction of composite materials for establishing impact tolerance. In this case, failure is assumed to initiate from a damage zone of material in the composite that can be approximated by an embedded crack. The time-dependent characteristics of the stresses for the through and embedded crack geometries are compared and studied for different elastic properties and dimensions of the composite. In particular, the phenomenon of elastic waves reflecting from the crack to the interfaces within the composite can be exhibited numerically when their neighboring boundaries are sufficiently close to one another. As time becomes very large, all of the results in this report reduce to the corresponding static solutions [4].

AXIAL SYMMETRIC DEFORMATION: PENNY-SHAPED CRACK

Consider a penny-shaped crack of radius a that lies in a layer of material of thickness $2b$ with material properties μ_1, ν_1, ρ_1 . This layer is bonded between two media with properties μ_2, ν_2, ρ_2 as illustrated in Figure 1. With reference to the system of coordinates (x,y,z) , the z -axis coincides with the center of the crack and is normal to the crack situated in the xy -plane. The outer boundaries of the composite are assumed to be sufficiently far away from the crack such that the reflected waves will have a negligible influence on the local stresses. Only those impact loads that produce an axisymmetric wave pattern will be considered.

For an axially symmetric deformation field, material elements are displaced only in the radial and axial direction and remain unchanged in the θ -direction. With reference to the cylindrical polar coordinates (r,θ,z) in Figure 1, the

two nonzero displacement components can be expressed in terms of the wave potentials $\phi_j(r,z,t)$ and $\psi_j(r,z,t)$ as follows:

$$(u_r)_j = \frac{\partial \phi_j}{\partial r} - \frac{\partial \psi_j}{\partial z} \quad (1)$$

$$(u_z)_j = \frac{\partial \phi_j}{\partial z} + \frac{\partial \psi_j}{\partial r} - \frac{\psi_j}{r}$$

where $j = 1$ refers to the layer with the crack and $j = 2$ to the surrounding material. The four nontrivial stress components are given by

$$\begin{aligned} (\sigma_r)_j &= 2\mu_j \frac{\partial}{\partial r} \left(\frac{\partial \phi_j}{\partial r} - \frac{\partial \psi_j}{\partial z} \right) + \lambda_j \nabla^2 \phi_j \\ (\sigma_\theta)_j &= 2\mu_j \frac{1}{r} \left(\frac{\partial \phi_j}{\partial r} - \frac{\partial \psi_j}{\partial z} \right) + \lambda_j \nabla^2 \phi_j \\ (\sigma_z)_j &= 2\mu_j \frac{\partial}{\partial z} \left(\frac{\partial \phi_j}{\partial z} + \frac{\partial \psi_j}{\partial r} + \frac{\psi_j}{r} \right) + \lambda_j \nabla^2 \phi_j \\ (\tau_{rz})_j &= \mu_j \left[\frac{\partial}{\partial z} \left(2 \frac{\partial \phi_j}{\partial r} - \frac{\partial \psi_j}{\partial z} \right) + \frac{\partial}{\partial r} \left(\frac{\partial \phi_j}{\partial r} + \frac{\psi_j}{r} \right) \right] \end{aligned} \quad (2)$$

in which λ_j and μ_j are the Lamé constants and ∇^2 represents the operator

$$\nabla^2 = \frac{\partial^2}{\partial r^2} + \frac{1}{r} \frac{\partial}{\partial r} + \frac{\partial^2}{\partial z^2}$$

The governing equations can thus be obtained from the equations of motion which yield

$$\frac{\partial^2 \phi_j}{\partial r^2} + \frac{1}{r} \frac{\partial \phi_j}{\partial r} + \frac{\partial^2 \phi_j}{\partial z^2} = \frac{1}{c_{1j}^2} \frac{\partial^2 \phi_j}{\partial t^2} \quad (3)$$

$$\frac{\partial^2 \psi_j}{\partial r^2} + \frac{1}{r} \frac{\partial \psi_j}{\partial r} - \frac{\psi_j}{r^2} + \frac{\partial^2 \psi_j}{\partial z^2} = \frac{1}{c_{2j}^2} \frac{\partial^2 \psi_j}{\partial t^2}$$

with c_{1j} and c_{2j} being the dilatational and shear wave speeds:

$$c_{1j} = \left(\frac{\lambda_j + 2\mu_j}{\rho_j} \right)^{1/2}, \quad c_{2j} = \left(\frac{\mu_j}{\rho_j} \right)^{1/2} \quad (4)$$

If the composite body is initially at rest, the Laplace transform of equations (3) further give

$$\frac{\partial^2 \phi_j^*}{\partial r^2} + \frac{1}{r} \frac{\partial \phi_j^*}{\partial r} + \frac{\partial^2 \phi_j^*}{\partial z^2} = \frac{p^2}{c_{1j}^2} \phi_j^* \quad (5)$$

$$\frac{\partial^2 \psi_j^*}{\partial r^2} + \frac{1}{r} \frac{\partial \psi_j^*}{\partial r} - \frac{\psi_j^*}{r^2} + \frac{\partial^2 \psi_j^*}{\partial z^2} = \frac{p^2}{c_{2j}^2} \psi_j^*$$

Here, p is the transform variable in the Laplace transform pair:

$$f^*(p) = \int_0^{\infty} f(t) \exp(-pt) dt \quad (6)$$

$$f(t) = \frac{1}{2\pi i} \int_{Br} f^*(p) \exp(pt) dp$$

The abbreviation Br stands for the Bromwich path of integration. Moreover, since the composite geometry is symmetrical about the xy-plane, it suffices to consider

only the solution in the upper half-space, $z \geq 0$. For the penny-shape crack geometry, the Hankel transform pair [5] may be used:

$$f^h(s) = \int_0^{\infty} xf(x) J_n(sx) dx$$

$$f(x) = \int_0^{\infty} sf^h(s) J_n(sx) ds$$
(7)

where J_n is the n th order Bessel function of the first kind. Applying equations (7) to (5), the following results are obtained:

$$\phi_1^*(r, z, p) = \int_0^{\infty} [A^{(1)}(s, p)e^{-\gamma_{11}z} + A^{(2)}(s, p)e^{\gamma_{11}z}] J_0(rs) ds$$

$$\psi_1^*(r, z, p) = \int_0^{\infty} [B^{(1)}(s, p)e^{-\gamma_{21}z} + B^{(2)}(s, p)e^{\gamma_{21}z}] J_1(rs) ds$$
(8)

for the cracked layer and

$$\phi_2^*(r, z, p) = \int_0^{\infty} C^{(1)}(s, p)e^{-\gamma_{12}z} J_0(rs) ds$$

$$\psi_2^*(r, z, p) = \int_0^{\infty} C^{(2)}(s, p)e^{-\gamma_{22}z} J_1(rs) ds$$
(9)

for the surrounding material. The quantities γ_{ij} are given by

$$\gamma_{1j} = \left(s^2 + \frac{p^2}{c_{1j}^2}\right)^{1/2}, \quad \gamma_{2j} = \left(s^2 + \frac{p^2}{c_{2j}^2}\right)^{1/2}$$
(10)

The six unknowns $A^{(1)}, A^{(2)}, \dots, C^{(2)}$ are determined from a given set of transient boundary, symmetry and continuity conditions.

NORMAL IMPACT

Let the penny-shaped crack be subjected to a uniform impact load* such that the upper and lower surface will move in the opposite direction. The magnitude of this normal load is σ_0 and since it is applied suddenly from $t = 0$ and maintained at a constant value thereafter, the Heaviside unit step function, $H(t)$, will be used, i.e., $-\sigma_0 H(t)$. Making use of equations (6), the conditions on the plane $z = 0$ for $r \leq a$ and $r \geq a$ take the forms

$$(\sigma_z^*)_1(r, 0, p) = -\frac{\sigma_0}{p}; (\tau_{rz}^*)_1(r, 0, p) = 0, 0 \leq r < a \quad (11)$$

$$(\sigma_z^*)_1(r, 0, p) = 0; (\tau_{rz}^*)_1(r, 0, p) = 0, r \geq a$$

If the interfaces at $z = \pm b$ is bonded perfectly, the stresses and displacements can then be considered continuous across these planes, i.e.,

$$(\sigma_z^*)_1(r, b, p) = (\sigma_z^*)_2(r, b, p) \quad (12)$$

$$(\tau_{rz}^*)_1(r, b, p) = (\tau_{rz}^*)_2(r, b, p)$$

*There is no loss in generality in formulating the problem in terms of a uniform step load. The principle of superposition may be used to obtain the solution for general loading from a series of step loading solutions as discussed in [1].

and

$$(u_r^*)_1(r,b,p) = (u_r^*)_2(r,b,p) \quad (13)$$

$$(u_z^*)_1(r,b,p) = (u_z^*)_2(r,b,p)$$

Under these considerations, the six functions $A^{(1)}, A^{(2)}, \dots, C^{(2)}$ may be expressed in terms of a single unknown $A(s,p)$ as indicated by equations (A.1) in the Appendix.

Fredholm integral equations. Without going into details, the function $A(s,p)$ can be obtained from the system of dual integral equations

$$\int_0^{\infty} A(s,p) J_0(rs) ds = 0, \quad r \geq a \quad (14)$$

$$\int_0^{\infty} s P_I(s,p) A(s,p) J_0(rs) ds = -\frac{\sigma_0}{2\mu_1(1-\kappa_1^2)p}, \quad r < a$$

in which $P_I(s,p)$ is a known function:

$$\begin{aligned} P_I(s,p) = & \frac{1}{s\Delta_I(1-\kappa_1^2)} \left\{ \left[\frac{1}{4} (s^2 + \gamma_{21}^2)^2 - s^2 \gamma_{11} \gamma_{21} \right] [\delta^{(2)} - \delta^{(3)} e^{-2(\gamma_{11} + \gamma_{21})b}] \right. \\ & + s(s^2 + \gamma_{21}^2) e^{-(\gamma_{11} + \gamma_{21})b} [\gamma_{21} (\delta^{(1)} \delta^{(4)} - \delta^{(2)} \delta^{(3)}) - \gamma_{11}] \\ & \left. + \left[\frac{1}{4} (s^2 + \gamma_{21}^2)^2 + s^2 \gamma_{11} \gamma_{21} \right] [\delta^{(4)} e^{-2\gamma_{21}b} - \delta^{(1)} e^{-2\gamma_{11}b}] \right\} \quad (15) \end{aligned}$$

The form of $A(s,p)$ that satisfies equations (14) can be found from Copson [6]:

$$A(s,p) = - \sqrt{\frac{2s}{\pi}} \frac{\sigma_0 a^{5/2}}{2\mu_1 p(1-\kappa_1^2)} \int_0^1 \sqrt{\xi} \Lambda_I^*(\xi,p) J_{1/2}(sa\xi) d\xi \quad (16)$$

Here, $J_{1/2}$ is the half order Bessel function of the first kind and $\Lambda_I^*(\xi,p)$ satisfies the Fredholm integral equation

$$\Lambda_I^*(\xi,p) + \int_0^1 \Lambda_I^*(\eta,p) M_I(\xi,\eta,p) d\eta = \xi \quad (17)$$

whose kernel

$$\begin{aligned} M_I(\xi,\eta,p) &= \sqrt{\xi\eta} \int_0^\infty s [P_I(\frac{s}{a},p) - 1] J_{1/2}(s\xi) J_{1/2}(s\eta) ds \\ &= \frac{2}{\pi} \int_0^\infty [P_I(\frac{s}{a},p) - 1] \sin(s\xi) \sin(s\eta) ds \end{aligned} \quad (18)$$

is symmetric in ξ and η . Figures 2 to 4 show the numerical results of equation (17) by varying μ_2/μ_1 and a/b while $\rho_1 = \rho_2$ and $\nu_1 = \nu_2 = 0.29$ are kept the same for all cases. The function $\Lambda_I^*(\xi,p)$ evaluated at the crack border, $\xi = 1$, governs the contribution of the geometric and material parameters on $k_1^*(p)$ which represents the Laplace transform of the stress intensity factor.

Stress intensity factor for normal impact. In order to evaluate $k_1^*(p)$ or $k_1(t)$, the stresses in the matrix layer are first expanded in terms of the local coordinates r_1 and θ_1 for small values of r_1 . The local coordinates (r_1, θ_1) are related to (r, θ) in Figure 1 as follows:

$$a + r_1 \cos \theta_1 = r \cos \theta \quad (19)$$

$$r_1 \sin \theta_1 = r \sin \theta$$

The leading term in the Laplace transform of the local stresses that possess the $1/\sqrt{r_1}$ singularity is

$$k_1^*(p) = \frac{\Lambda_I^*(1,p)}{p} \frac{2}{\pi} \sigma_0 \sqrt{a} \quad (20)$$

Application of the Laplace inversion theorem yields the dynamic stress field around the crack border as a function of time. The result is

$$\begin{aligned} (\sigma_r)_1(r_1, \theta_1, t) &= \frac{k_1(t)}{\sqrt{2r_1}} \cos \frac{\theta_1}{2} \left(1 - \sin \frac{\theta_1}{2} \sin \frac{3\theta_1}{2}\right) + O(r_1^0) \\ (\sigma_\theta)_1(r_1, \theta_1, t) &= \frac{k_1(t)}{\sqrt{2r_1}} 2\nu_1 \cos \frac{\theta_1}{2} + O(r_1^0) \\ (\sigma_z)_1(r_1, \theta_1, t) &= \frac{k_1(t)}{\sqrt{2r_1}} \cos \frac{\theta_1}{2} \left(1 + \sin \frac{\theta_1}{2} \sin \frac{3\theta_1}{2}\right) + O(r_1^0) \\ (\tau_{rz})_1(r_1, \theta_1, t) &= \frac{k_1(t)}{\sqrt{2r_1}} \cos \frac{\theta_1}{2} \sin \frac{\theta_1}{2} \cos \frac{3\theta_1}{2} + O(r_1^0) \end{aligned} \quad (21)$$

and $k_1(t)$ becomes

$$k_1(t) = \frac{2\sigma_0\sqrt{a}}{\pi} \frac{1}{2\pi i} \int_{Br} \frac{\Lambda_I^*(1,p)}{p} e^{pt} dp \quad (22)$$

Note that equation (20) is, in fact, the Laplace transform of equation (22). Hence, the functional dependence of r_1 and θ_1 is not affected by the Laplace

transformation and can be evaluated separately. This observation was first made by Sih, Ravera and Embley [7].

Making use of the results for $\Lambda_I^*(1,p)$ in Figures 2 to 4, $k_1(t)$ in equation (22) can be found as given in Figures 5 to 7. The dynamic stress intensity factors $k_1(t)$ for the penny-shaped crack exhibit an oscillatory behavior rising quickly to a peak. As time increases, all curves approach the static value of $k_1 = 2\sigma_0\sqrt{a}/\pi$ [4]. For a crack diameter to layer thickness ratio of $a/b = 1$, the peaks of the $k_1(t)$ curve are sensitive to changes in the shear moduli ratio μ_2/μ_1 . Figure 5 indicates that $k_1(t)$ tends to decrease in amplitude as μ_2/μ_1 is reduced from 0.1 to 10.0. The influence of the composite interface on $k_1(t)$ is exhibited in Figures 6 to 7. When the shear modulus of the surrounding material μ_2 is much smaller than the matrix layer with μ_1 , the dynamic crack border stress intensity increases as the crack diameter becomes large in comparison with the layer thickness. This effect is clearly evidenced in Figure 6. As expected, $k_1(t)$ increases with decreasing a/b when the shear modulus of the cracked layer is made smaller than the surrounding material, i.e., $\mu_1 < \mu_2$ as illustrated in Figure 7. The result of Embley and Sih [8] is recovered for the homogeneous case, $\mu_1 = \mu_2$.

RADIAL IMPACT

If the penny-shaped crack is sheared uniformly in the radial direction such that axial symmetry is preserved, then $\phi_j^*(r,z,p)$ and $\psi_j^*(r,z,p)$ in equations (8) and (9) remain valid. Let this shear of magnitude τ_0 be applied suddenly and hence the surface tractions, $-\tau_0 H(t)$, are to be specified for $0 \leq r < a$ with $H(t)$ being the Heaviside unit step function. Laplace transform of the conditions on the plane $z = 0$ thus become

$$(\tau_{rz}^*)_1(r,0,p) = -\frac{\tau_0}{p}; (\sigma_z^*)_1(r,0,p) = 0, 0 \leq r < a$$
(23)

$$(u_r^*)_1(r,0,p) = 0; (\sigma_z^*)_1(r,0,p) = 0, r \geq a$$

Continuity of the stresses across the interface $z = b$ is satisfied if

$$(\sigma_z^*)_1(r,b,p) = (\sigma_z^*)_2(r,b,p)$$
(24)

$$(\sigma_{rz}^*)_1(r,b,p) = (\sigma_{rz}^*)_2(r,b,p)$$

and the same requirement is imposed on the displacements:

$$(u_r^*)_1(r,b,p) = (u_r^*)_2(r,b,p)$$
(25)

$$(u_z^*)_1(r,b,p) = (u_z^*)_2(r,b,p)$$

Integral equations. As in the case of normal impact, the six unknown functions $A^{(1)}(s,p)$, $A^{(2)}(s,p), \dots, C^{(2)}(s,p)$ in equations (8) and (9) can be expressed in terms of a single unknown $B(s,p)$. Refer to equations (A.5) in the Appendix. Hence, equations (24) and (25) are satisfied. The remaining boundary conditions in equations (23) are employed to obtain the system of dual integral equations

$$\int_0^{\infty} B(s,p) J_1(rs) ds = 0, \quad r \geq a \quad (26)$$

$$\int_0^{\infty} s P_{II}(s,p) B(s,p) J_1(rs) ds = - \frac{\tau_0}{2\mu_1(1-\kappa_1^2)p}, \quad r < a$$

in which

$$P_{II}(s,p) = \frac{\Delta_I}{\Delta_{II}} P_I(s,p) \quad (27)$$

where $P_I(s,p)$ is already known through equation (15) while $\Delta_I(s,p)$ and $\Delta_{II}(s,p)$ are given by equations (A.2) and (A.6), respectively.

Solving for $B(s,p)$ [6], it can be shown that

$$B(s,p) = - \sqrt{\frac{\pi s}{2}} \frac{\tau_0 a^{5/2}}{4\mu_1 p(1-\kappa_1^2)} \int_0^1 \sqrt{\xi} \Lambda_{II}^*(\xi,p) J_{3/2}(sa\xi) d\xi \quad (28)$$

and $\Lambda_{II}^*(\xi,p)$ satisfies the Fredholm integral equation of the second kind:

$$\Lambda_{II}^*(\xi,p) + \int_0^1 \Lambda_{II}^*(\eta,p) M_{II}(\xi,\eta,p) d\eta = \xi \quad (29)$$

whose kernel takes the form

$$M_{II}(\xi,\eta,p) = \sqrt{\xi\eta} \int_0^{\infty} s [P_{II}(\frac{s}{a}, p) - 1] J_{3/2}(s\xi) J_{3/2}(s\eta) ds \quad (30)$$

Plots of $\Lambda_{II}^*(1,p)$ as a function of c_{21}/pa are shown in Figures 8 to 10 for different values of μ_2/μ_1 and a/h . The curves show that $\Lambda_{II}^*(1,p)$ rises rapidly at first and then levels off.

Stress intensity factor for radial impact. The dynamic crack border stress field corresponding to radial shear can be obtained in the same way and expressed in terms of the coordinates (r_1, θ_1) in equations (19):

$$\begin{aligned}
 (\sigma_r)_1(r_1, \theta_1, t) &= \frac{k_2(t)}{\sqrt{2r_1}} \sin \frac{\theta_1}{2} \left(2 + \cos \frac{\theta_1}{2} \cos \frac{3\theta_1}{2} \right) + O(r_1^0) \\
 (\sigma_\theta)_1(r_1, \theta_1, t) &= \frac{k_2(t)}{\sqrt{2r_1}} 2\nu_1 \sin \frac{\theta_1}{2} + O(r_1^0) \\
 (\sigma_z)_1(r_1, \theta_1, t) &= -\frac{k_2(t)}{\sqrt{2r_1}} \sin \frac{\theta_1}{2} \cos \frac{\theta_1}{2} \cos \frac{3\theta_1}{2} + O(r_1^0) \\
 (\tau_{rz})_1(r_1, \theta_1, t) &= \frac{k_2(t)}{\sqrt{2r_1}} \cos \frac{\theta_1}{2} \left(1 - \sin \frac{\theta_1}{2} \sin \frac{3\theta_1}{2} \right) + O(r_1^0)
 \end{aligned} \tag{31}$$

Note that $k_2(t)$ can be evaluated from

$$k_2(t) = \frac{\tau_0 \sqrt{a}}{4\pi i} \int_{Br} \frac{\Lambda_{II}^*(1, p)}{p} e^{pt} dp \tag{32}$$

once $\Lambda_{II}^*(1, p)$ as given by Figures 8 to 10 is known.

The numerical results in Figures 11 to 13 for $k_2(t)$ as a function of time refer to $\rho_1 = \rho_2$ and $\nu_1 = \nu_2 = 0.29$. The curve with $\mu_1 = \mu_2$ is the solution for the homogeneous material treated previously by Embley and Sih [8]. In general, $k_2(t)$ oscillates with time and can be greater or smaller than the corresponding homogeneous solution depending on whether $\mu_2/\mu_1 < 1$ or $\mu_2/\mu_1 > 1$. Figure 11 displays the variations of $k_2(t)$ for different values of μ_2/μ_1 while a/b is fixed at unity. The influence of the ratio of crack size with layer thickness

is exhibited in Figures 12 and 13 for $\mu_2/\mu_1 = 0.1$ and $\mu_2/\mu_1 = 10.0$, respectively. These two cases show the opposite effect which is to be expected.

CONCLUDING REMARKS

The previous discussion has shown that the dynamic stress intensity factors for an embedded crack can be evaluated analytically by a method similar to that developed for a through crack [1]. An important consideration is to compare the results for these two crack configurations and to draw some general conclusions. First of all, the $k_1(t)$ or $k_2(t)$ factor for the penny-shaped crack tends to rise more quickly than the through crack, i.e., the peak value of $k_1(t)$ or $k_2(t)$ is reached within a shorter period of time. This is because waves emanating from the neighboring points on the periphery of the penny-shaped crack interfere with each other much earlier as compared to a line (or plane) crack where the waves must travel from one end to the other before interference can take place. In general, the maximum value of $k_1(t)$ or $k_2(t)$ for an embedded crack is lower than that for a through crack. For example, Figure 5 gives a peak value of approximately 1.6 for $\pi k_1(t)/2\sigma_0\sqrt{a}$ which corresponds to $a/b = 1.0$ and $\mu_2/\mu_1 = 0.1$. This occurs at $c_{21}t/a \approx 1.6$ and yields $k_1(t) \approx 1.02 \sigma_0\sqrt{a}$. The corresponding case of a through crack [1] renders $k_1(t) \approx 2.40 \sigma_0\sqrt{a}$ and $c_{21}t/a \approx 3.0$. The difference in $k_1(t)$ is more than a factor of two and is more pronounced as the ratio a/b is increased. For embedded cracks that are non-circular in shape, approximate estimates of $k_1(t)$ can be made by taking the solution for the through crack as an upper limit and that of the circular crack as a lower limit.

In the absence of axisymmetry, the dynamic stress analysis will become exceedingly difficult and it will be more feasible to solve the crack problem numerically. In such cases, the solutions obtained here can be used to guide the development of numerical procedures.

APPENDIX: EXPRESSIONS FOR $A^{(i)}(s,p), \dots, C^{(i)}(s,p)$

Normal impact. The functions $A^{(1)}(s,p), A^{(2)}(s,p), \dots, C^{(2)}(s,p)$ for the wave potentials in equations (8) and (9) can be expressed in terms of a single unknown $A(s,p)$ for normal impact

$$A^{(1)}(s,p) = \left[\frac{1}{2} (s^2 + \gamma_{21}^2) (\delta^{(2)} + \delta^{(4)} e^{-2\gamma_{21}b}) - s\gamma_{11} e^{-(\gamma_{11} + \gamma_{21})b} \right] \frac{A(s,p)}{\Delta_I}$$

$$A^{(2)}(s,p) = - \left[s\gamma_{11} e^{-(\gamma_{11} + \gamma_{21})b} + \frac{1}{2} (s^2 + \gamma_{21}^2) e^{-2\gamma_{11}b} (\delta^{(1)} + \delta^{(3)} e^{-2\gamma_{21}b}) \right] \times \frac{A(s,p)}{\Delta_I}$$

$$B^{(1)}(s,p) = - \left[\delta^{(1)} A^{(1)} e^{-\gamma_{11}b} + \delta^{(2)} A^{(2)} e^{\gamma_{11}b} \right]$$

$$B^{(2)}(s,p) = - \left[\delta^{(3)} A^{(1)} e^{-\gamma_{11}b} + \delta^{(4)} A^{(2)} e^{\gamma_{11}b} \right] \quad (A.1)$$

$$C^{(1)}(s,p) = \frac{e^{\gamma_{12}b}}{s^2 - \gamma_{12}\gamma_{22}} \left[(s^2 - \gamma_{11}\gamma_{22}) A^{(1)} e^{-\gamma_{11}b} + (s^2 + \gamma_{11}\gamma_{22}) A^{(2)} e^{\gamma_{11}b} - s(\gamma_{21} - \gamma_{22}) B^{(1)} e^{-\gamma_{21}b} + s(\gamma_{21} + \gamma_{22}) B^{(2)} e^{\gamma_{21}b} \right]$$

$$C^{(2)}(s,p) = \frac{e^{\gamma_{22}b}}{s^2 - \gamma_{12}\gamma_{22}} \left[s(\gamma_{12} - \gamma_{11}) A^{(1)} e^{-\gamma_{11}b} + s(\gamma_{11} + \gamma_{12}) e^{\gamma_{11}b} + (s^2 - \gamma_{21}\gamma_{12}) B^{(1)} e^{-\gamma_{21}b} + (s^2 + \gamma_{21}\gamma_{12}) B^{(2)} e^{\gamma_{21}b} \right]$$

in which Δ_I stands for

$$\Delta_I(s,p) = \frac{p^2}{2c_{21}^2} \gamma_{11} [\delta^{(2)} + \delta^{(3)} e^{-2(\gamma_{11} + \gamma_{21})b} + \delta^{(4)} e^{-2\gamma_{21}b} + \delta^{(1)} e^{-2\gamma_{11}b}] \quad (\text{A.2})$$

and $\delta^{(1)}, \delta^{(2)}, \dots, \delta^{(4)}$ are further expressed in terms of $e^{(1)}, e^{(2)}, \dots, e^{(8)}$ as the following:

$$\begin{aligned} \delta^{(1)}(s,p) &= (e^{(1)}e^{(6)} - e^{(2)}e^{(7)}) / (e^{(1)}e^{(6)} - e^{(2)}e^{(5)}) \\ \delta^{(2)}(s,p) &= (e^{(4)}e^{(6)} - e^{(2)}e^{(8)}) / (e^{(1)}e^{(6)} - e^{(2)}e^{(5)}) \\ \delta^{(3)}(s,p) &= (e^{(1)}e^{(7)} - e^{(3)}e^{(5)}) / (e^{(1)}e^{(6)} - e^{(2)}e^{(5)}) \\ \delta^{(4)}(s,p) &= (e^{(1)}e^{(8)} - e^{(4)}e^{(5)}) / (e^{(1)}e^{(6)} - e^{(2)}e^{(5)}) \end{aligned} \quad (\text{A.3})$$

The quantities in equations (A.3) are complicated functions of the materials parameters and transform variables. They are given by

$$\begin{aligned} e^{(1)}(s,p) &= -s\gamma_{21} + \frac{s\mu_2}{\mu_1(s^2 - \gamma_{12}\gamma_{22})} \left[\frac{1}{2} (\gamma_{21} - \gamma_{22})(s^2 + \gamma_{22}^2) + \gamma_{22}(s^2 - \gamma_{21}\gamma_{12}) \right] \\ e^{(2)}(s,p) &= s\gamma_{21} - \frac{s\mu_2}{\mu_1(s^2 - \gamma_{12}\gamma_{22})} \left[\frac{1}{2} (\gamma_{21} + \gamma_{22})(s^2 + \gamma_{22}^2) - \gamma_{22}(s^2 + \gamma_{21}\gamma_{12}) \right] \\ e^{(3)}(s,p) &= \frac{1}{2} (s^2 + \gamma_{21}^2) - \frac{\mu_2}{\mu_1(s^2 - \gamma_{12}\gamma_{22})} \left[\frac{1}{2} (s^2 + \gamma_{22}^2)(s^2 - \gamma_{11}\gamma_{22}) \right. \\ &\quad \left. + s^2\gamma_{22}(\gamma_{11} - \gamma_{12}) \right] \end{aligned}$$

$$e^{(4)}(s,p) = \frac{1}{2} (s^2 + \gamma_{21}^2) - \frac{\mu_2}{\mu_1 (s^2 - \gamma_{12} \gamma_{22})} \left[\frac{1}{2} (s^2 + \gamma_{22}^2) (s^2 + \gamma_{11} \gamma_{22}) \right. \\ \left. - s^2 \gamma_{22} (\gamma_{11} + \gamma_{12}) \right]$$

$$e^{(5)}(s,p) = -\frac{1}{2} (s^2 + \gamma_{21}^2) + \frac{\mu_2}{\mu_1 (s^2 - \gamma_{12} \gamma_{22})} \left[s^2 \gamma_{12} (\gamma_{21} - \gamma_{22}) \right. \\ \left. + \frac{1}{2} (s^2 + \gamma_{22}^2) (s^2 - \gamma_{21} \gamma_{12}) \right]$$

(A.4)

$$e^{(6)}(s,p) = -\frac{1}{2} (s^2 + \gamma_{21}^2) - \frac{\mu_2}{\mu_1 (s^2 - \gamma_{12} \gamma_{22})} \left[s^2 \gamma_{12} (\gamma_{21} + \gamma_{22}) \right. \\ \left. - \frac{1}{2} (s^2 + \gamma_{22}^2) (s^2 + \gamma_{21} \gamma_{12}) \right]$$

$$e^{(7)}(s,p) = s \gamma_{11} - \frac{s \mu_2}{\mu_1 (s^2 - \gamma_{12} \gamma_{22})} \left[\gamma_{12} (s^2 - \gamma_{11} \gamma_{22}) + \frac{1}{2} (s^2 + \gamma_{22}^2) (\gamma_{11} - \gamma_{12}) \right]$$

$$e^{(8)}(s,p) = -s \gamma_{11} - \frac{s \mu_2}{\mu_1 (s^2 - \gamma_{12} \gamma_{22})} \left[\gamma_{12} (s^2 + \gamma_{11} \gamma_{22}) - \frac{1}{2} (s^2 + \gamma_{22}^2) (\gamma_{11} + \gamma_{12}) \right]$$

Radial impact. For radial impact, $A^{(1)}(s,p)$, $A^{(2)}(s,p)$, ..., $C^{(2)}(s,p)$ in equations (8) and (9) can be expressed in terms of $B(s,p)$ as

$$A^{(1)}(s,p) = - \left[s \gamma_{21} (\delta^{(2)} - \delta^{(4)} e^{-2\gamma_{21} b}) + \frac{1}{2} (s^2 + \gamma_{21}^2) e^{-(\gamma_{11} + \gamma_{21}) b} \right] \frac{B(s,p)}{\Delta_{II}}$$

(A.5)

$$A^{(2)}(s,p) = \left[s \gamma_{21} e^{-2\gamma_{11} b} (\delta^{(1)} - \delta^{(3)} e^{-2\gamma_{21} b}) + \frac{1}{2} (s^2 + \gamma_{21}^2) e^{-(\gamma_{11} + \gamma_{21}) b} \right] \\ \times \frac{B(s,p)}{\Delta_{II}}$$

where

$$\Delta_{II} = \frac{p^2}{2c_{21}^2} \gamma_{21} [\delta^{(2)} + \delta^{(3)} e^{-2(\gamma_{11} + \gamma_{21})b} - \delta^{(4)} e^{-2\gamma_{21}b} - \delta^{(1)} e^{-2\gamma_{11}b}] \quad (A.6)$$

The remaining functions $B^{(1)}(s,p)$, $B^{(2)}(s,p)$, etc., can be related to $B(s,p)$ through $A^{(1)}(s,p)$ and $A^{(2)}(s,p)$ since the last four expressions in equations (A.1) for normal impact also apply to radial impact.

ACKNOWLEDGEMENTS

The authors wish to acknowledge the financial support provided by the National Aeronautics and Space Administration, Lewis Research Center, Cleveland, Ohio under Contract No. NSG-3179 with the Institute of Fracture and Solid Mechanics, Lehigh University. They are also grateful to Dr. C. C. Chamis for having expressed an interest in this work.

REFERENCES

- [1] Sih, G. C. and Chen, E. P., "Angle Impact of Unidirectional Composites with Cracks: Dynamic Stress Intensification", Technical Report IFSM No. 95, Lehigh University, January, 1979.
- [2] Lauraitis, K., "Tensile Strength of Off-Axis Unidirectional Composites", University of Illinois TAM Report No. 344, 1971.
- [3] Sih, G. C., "Dynamic Crack Problems: Strain Energy Density Fracture Theory", Mechanics of Fracture, Vol. IV, edited by G. C. Sih, Sijthoff and Noordhoff International Publishing, Alphen, pp. XVII-XLVII, 1977.

- [4] "Three-Dimensional Crack Problems", Mechanics of Fracture, Vol. II, edited by G. C. Sih, Sijthoff and Noordhoff International Publishing, Alphen, Chapter 1, 1975.
- [5] Sneddon, I. N., Fourier Transforms, McGraw-Hill, New York, 1958.
- [6] Copson, E. T., "On Certain Dual Integral Equations", Proceedings of Glasgow Mathematical Association, Vol. 5, pp. 19-24, 1961.
- [7] Sih, G. C., Ravera, R. S. and Embley, G. T., "Impact Response of a Finite Crack in Plane Extension", International Journal of Solids and Structures, Vol. 8, pp. 977-993, 1972.
- [8] Embley, G. T. and Sih, G. C., "Response of a Penny-Shaped Crack to Impact Waves", Proceedings of the 12th Midwestern Mechanics Conference, Vol. 6, pp. 473-487, 1971.

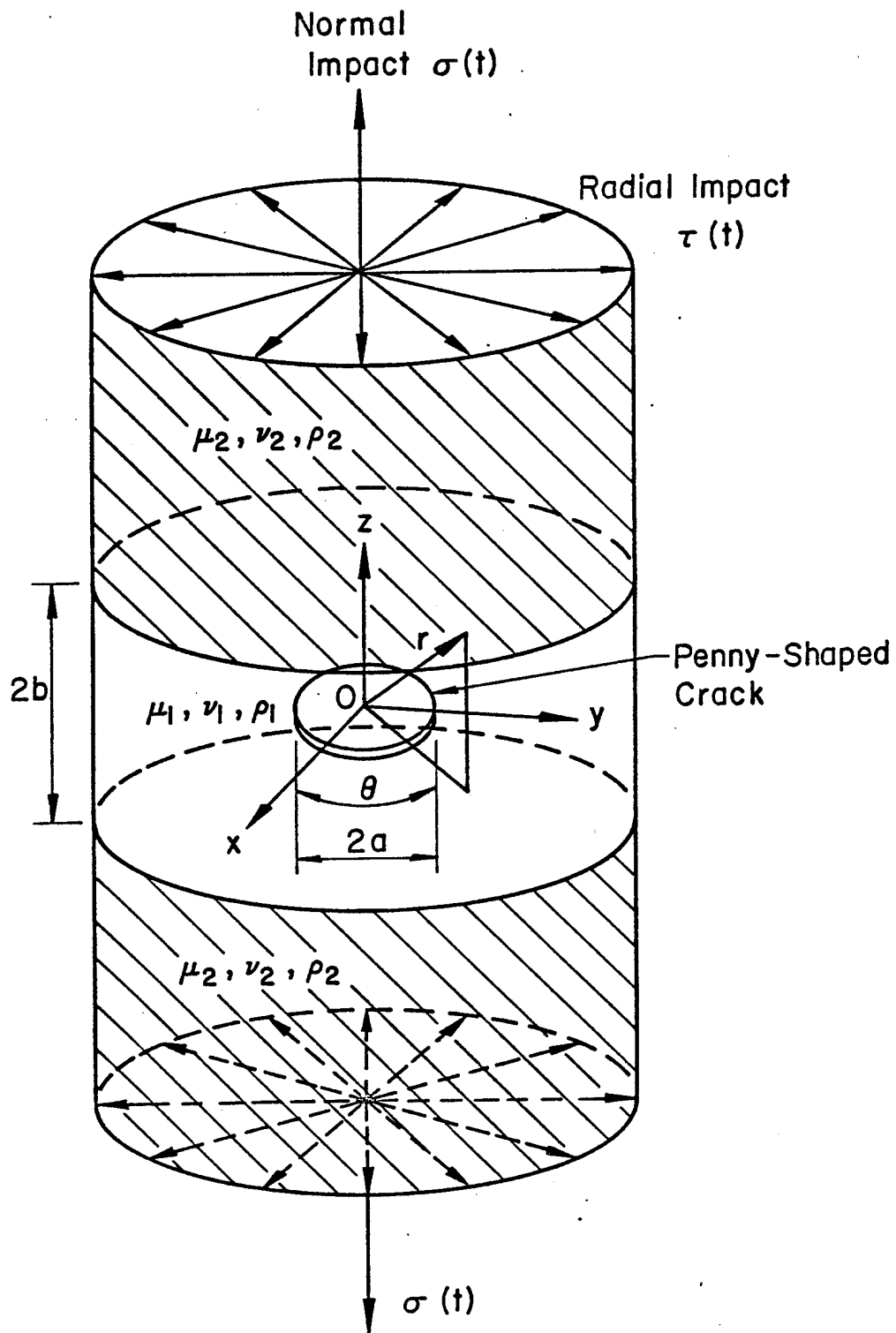


Figure 1 - Penny-shaped crack embedded in a matrix layer under normal and radial impact

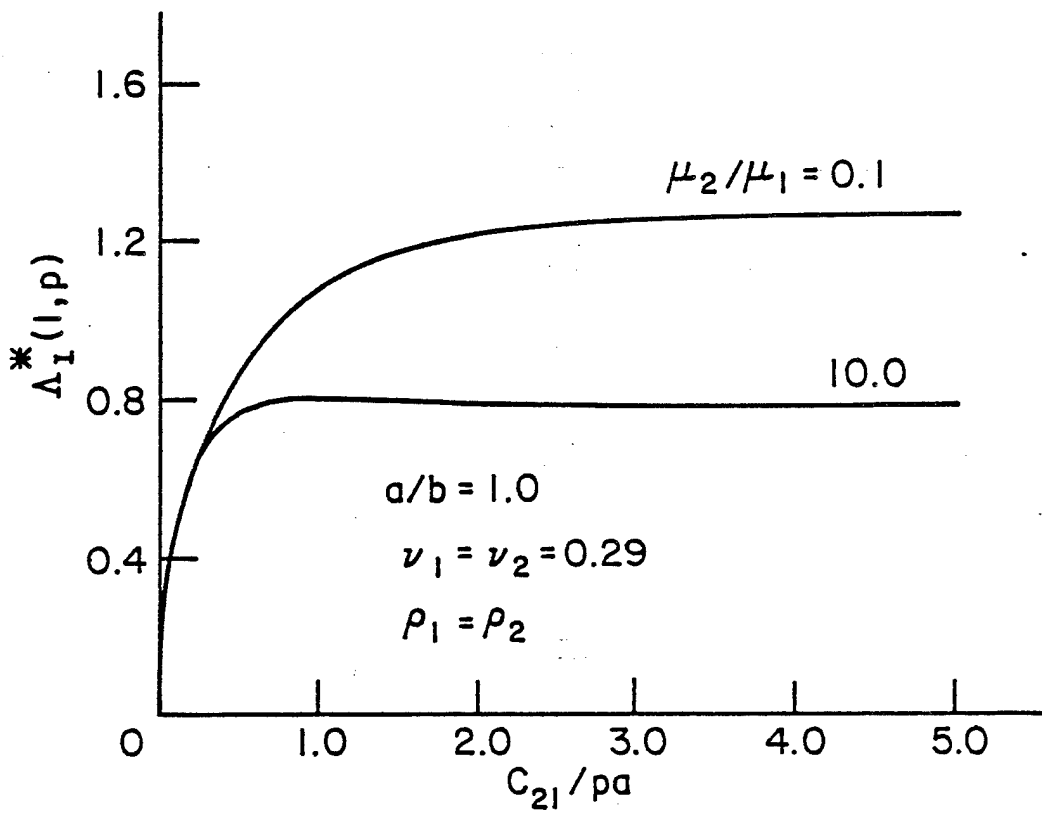


Figure 2 - Plot of $\Delta_I^*(1, \rho)$ versus c_{21}/pa for $a/b = 1.0$

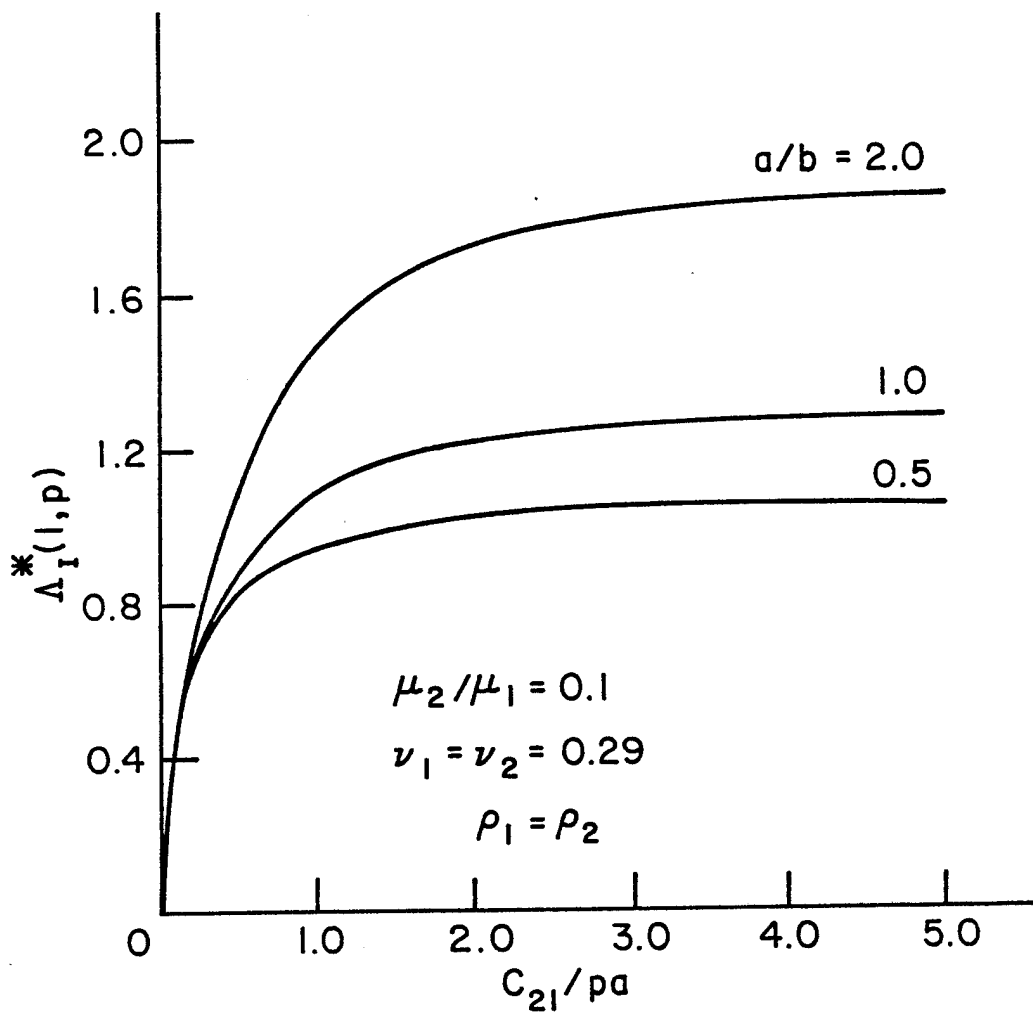


Figure 3 - Plot of $\Delta_I^*(1,p)$ versus c_{21}/pa for $\mu_2/\mu_1 = 0.1$

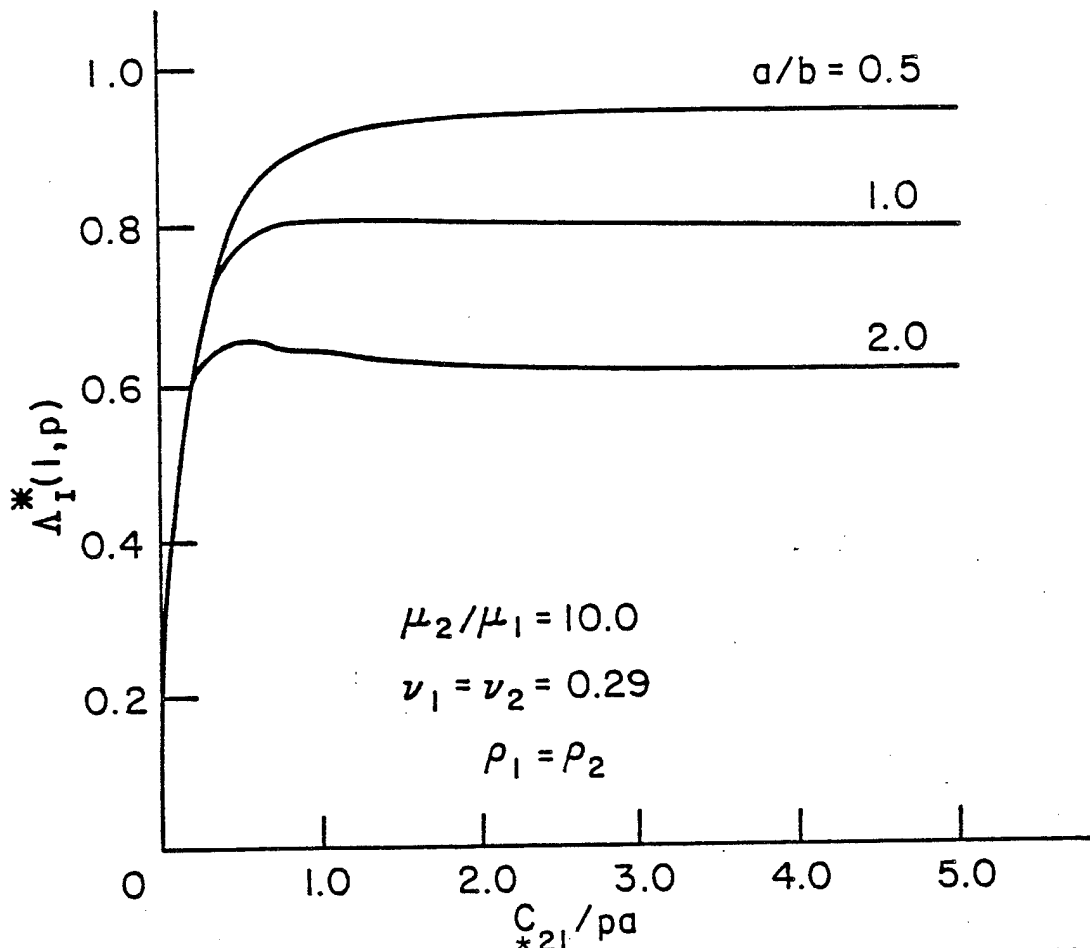


Figure 4 - Plot of $\Delta_I^*(l,p)$ versus c_{2l}/pa for $\mu_2/\mu_1 = 10.0$

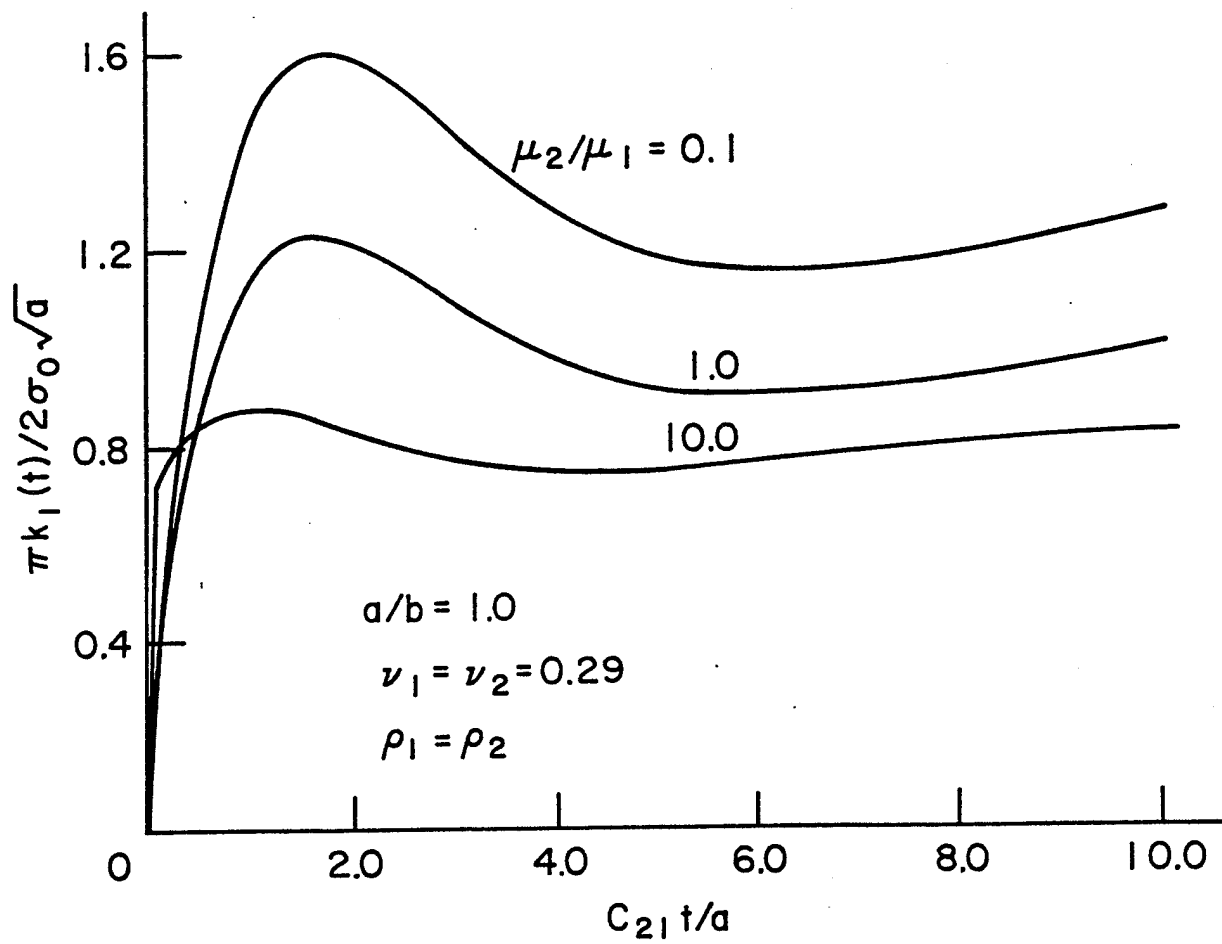


Figure 5 - Dynamic stress intensity factor $k_1(t)$ for penny-shaped crack with $a/b = 1.0$

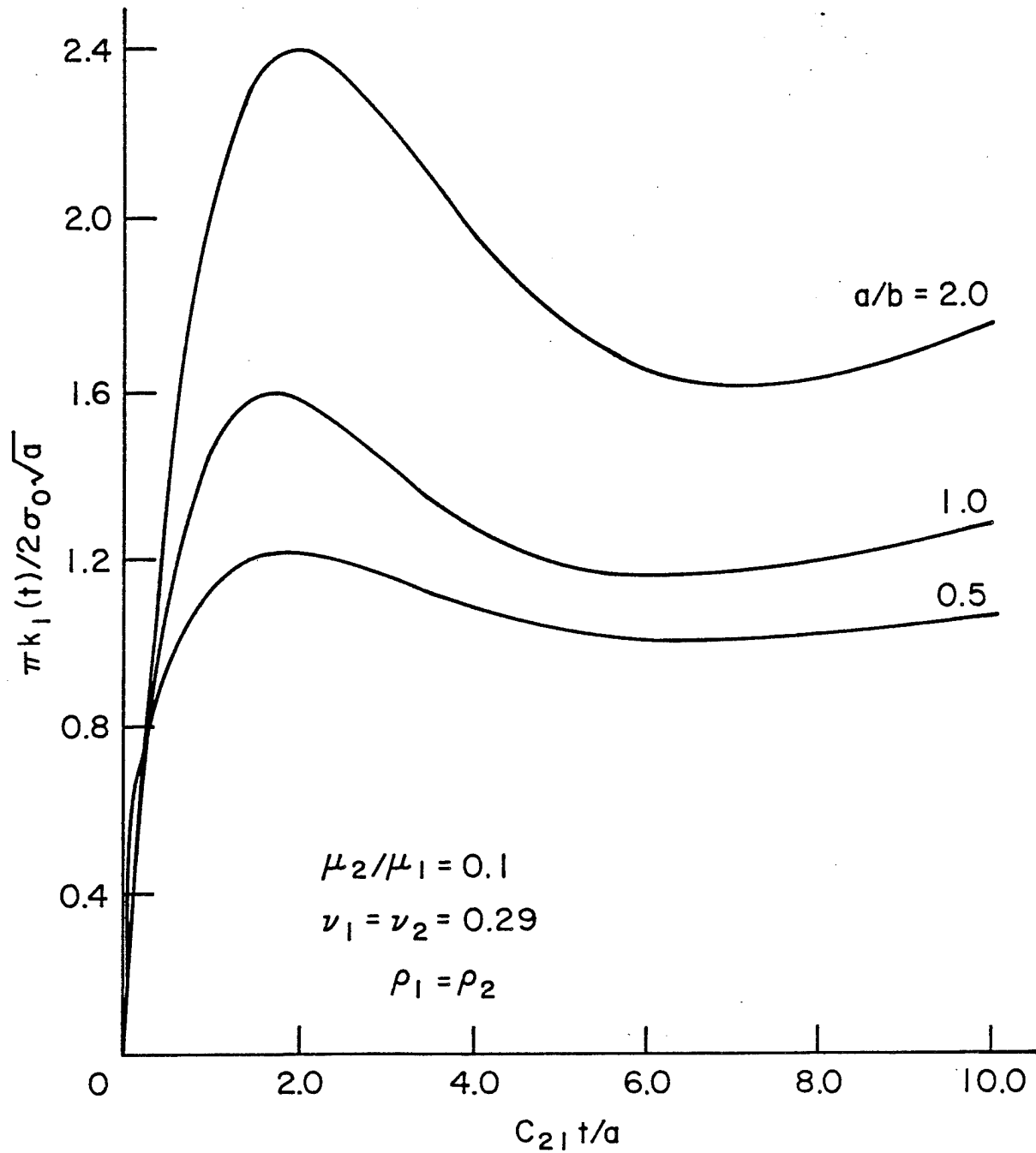


Figure 6 - Dynamic stress intensity factor $k_1(t)$ for penny-shaped crack with $\mu_2/\mu_1 = 0.1$

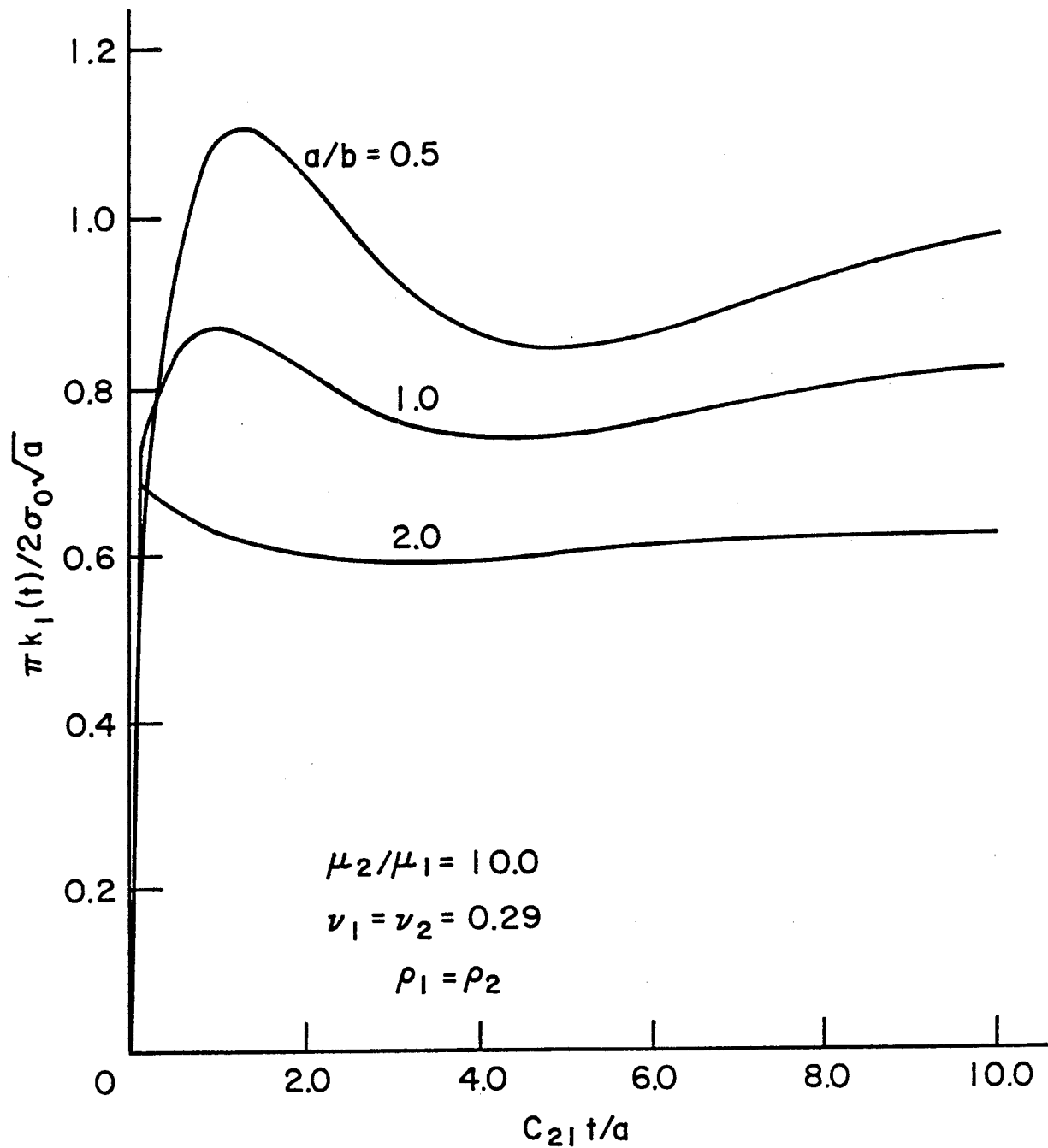


Figure 7 - Dynamic stress intensity factor $k_1(t)$ for penny-shaped crack with $\mu_2/\mu_1 = 10.0$

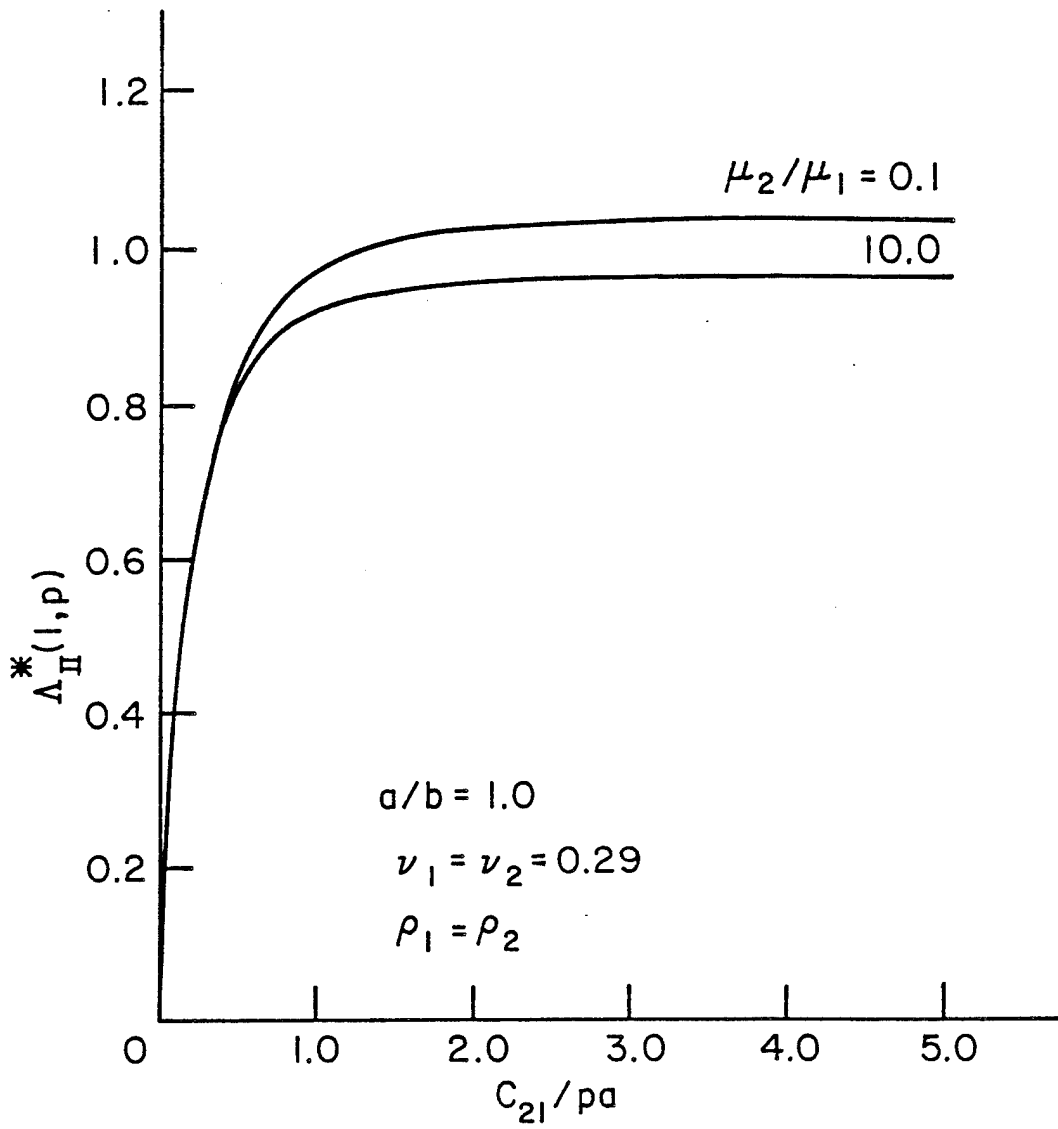


Figure 8 - Variations of $\Lambda_{II}^*(1,p)$ with c_{21}/pa for $a/b = 1.0$

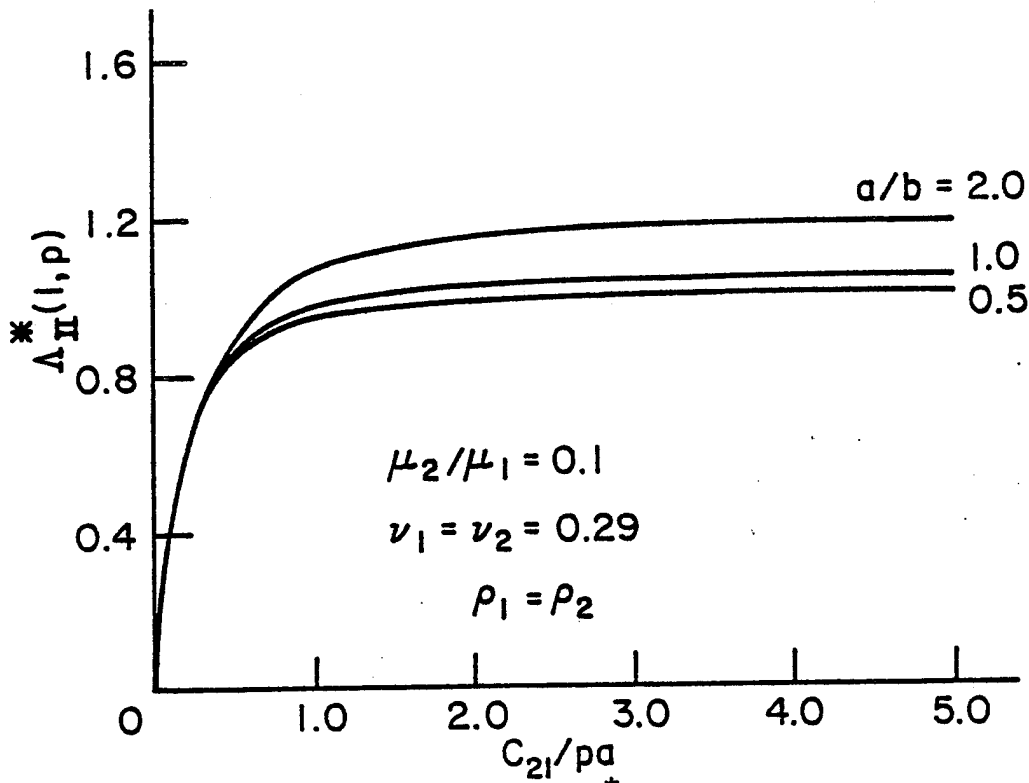


Figure 9 - Variations of $\Delta_{II}^*(1, p)$ with c_{21}/pa for $\mu_2/\mu_1 = 0.1$ and varying a/b

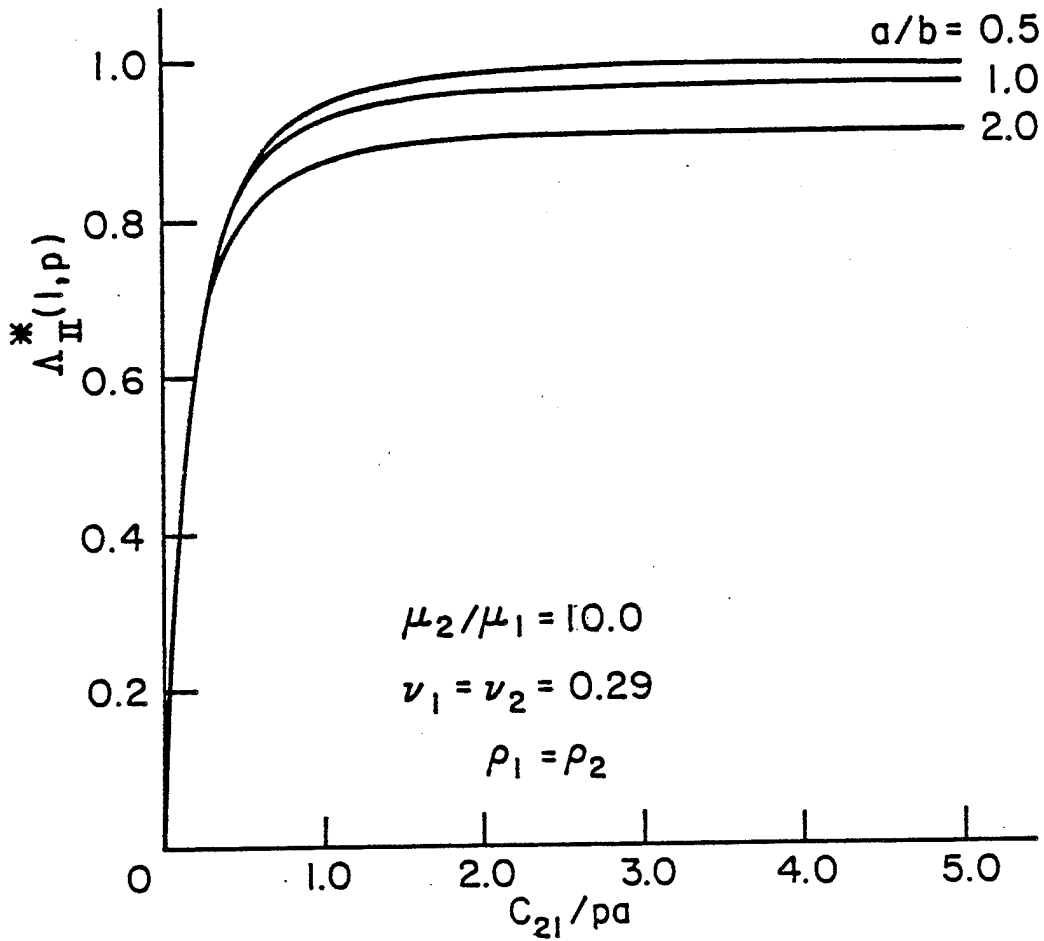


Figure 10 - Variations of $\Lambda_{II}^*(1,p)$ with c_{21}/pa for $\mu_2/\mu_1 = 10$ and varying a/b

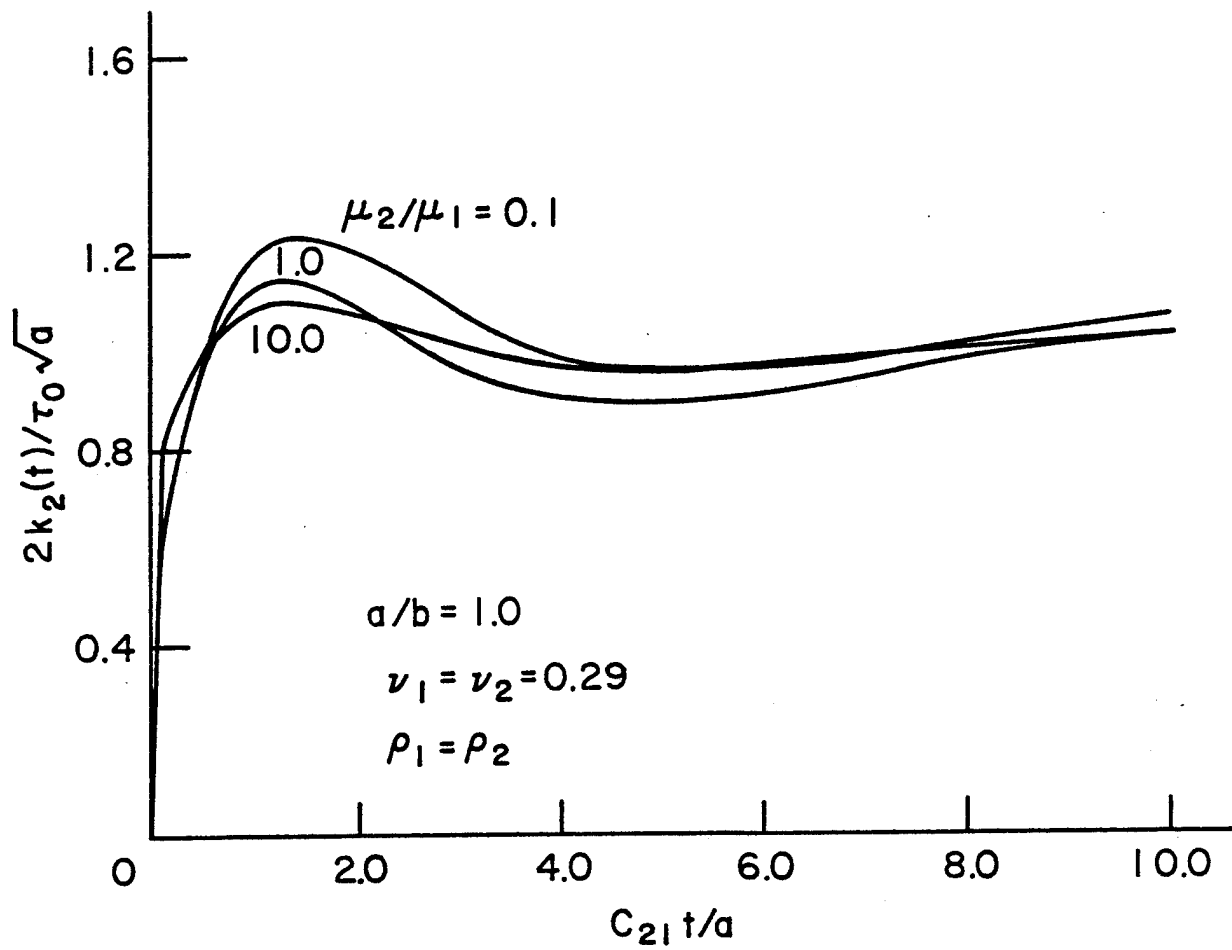


Figure 11 - Stress intensity factor $k_2(t)$ versus time for a penny-shaped crack with $a/b = 1.0$

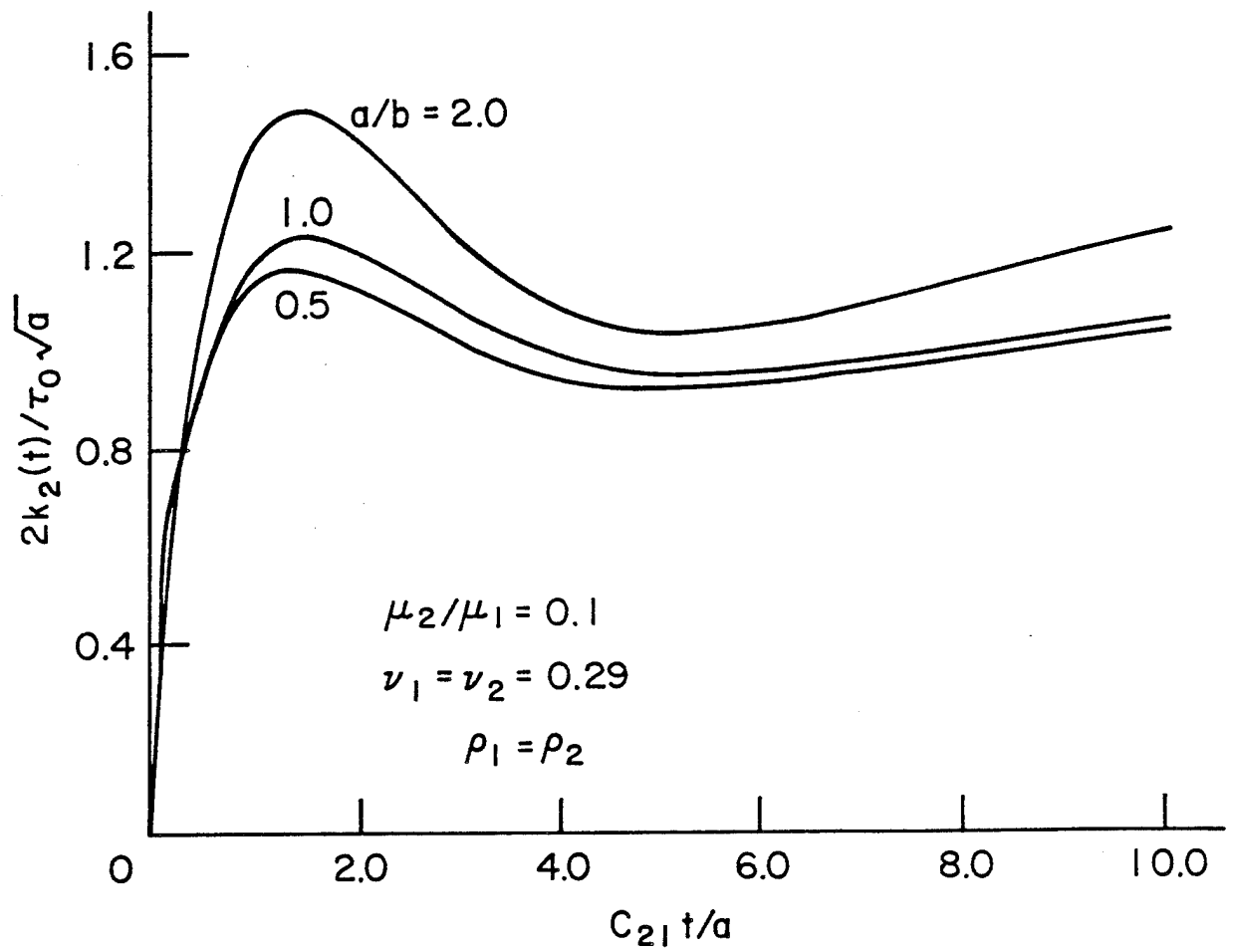


Figure 12 - Stress intensity factor $k_2(t)$ versus time for a penny-shaped crack with $\mu_2/\mu_1 = 0.1$

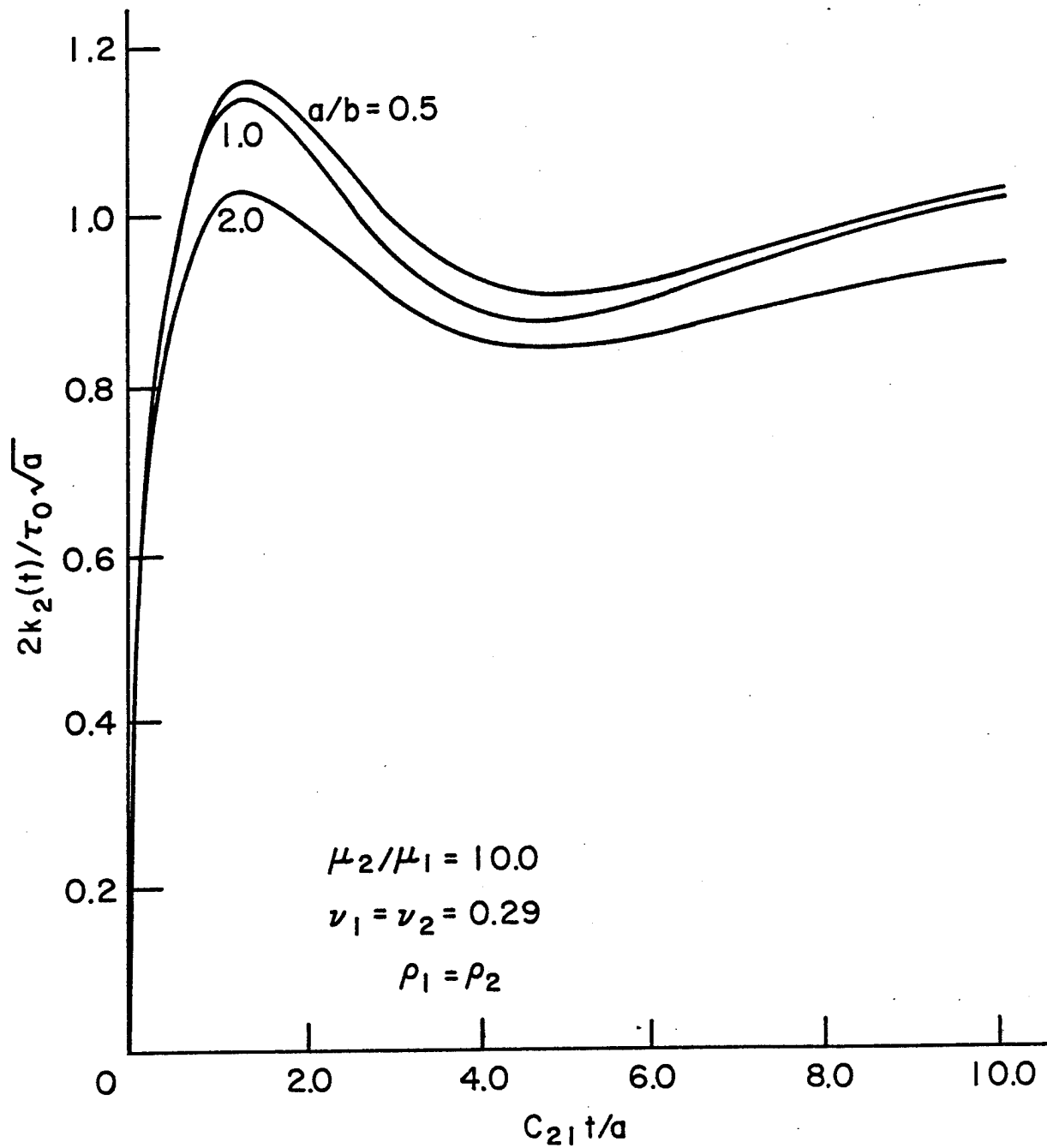


Figure 13 - Stress intensity factor $k_2(t)$ versus time for a penny-shaped crack with $\mu_2/\mu_1 = 10.0$

Axial Impact

```

PROGRAM BETA(INPUT,OUTPUT,PUNCH,PLOT,TAPE 99=PLOT)
3 REAL NON(4),F(4,4,1),G(4,4),D(4),PT(4)
3 REAL B(4),C(4)
3 REAL LP(50),DTA(50)
3 EQUIVALENCE (NON,B)
3 COMMON K1,K2,K3,K4
3 COMMON/AUX/H,P,PK1,PK2,BMU,X,Y
3 LP(1)=0.0
4 DTA(1)=0.0
5 READ 2,K1,K2,K3,K4
20 2 FORMAT(I2)
* K1 = ORDER OF SYSTEM OF EQUATIONS
* K2 = NO. OF DISTINCT KERNELS
* K3 = NO. OF DATA POINTS
* K4 = NO. OF DATA SETS TO BE EVALUATED
* SET UP DATA POINTS
20 AK=K3
22 DO 5 N=1,K3
23 AN=N
24 5 PT(N)=AN/AK
* SET UP INTEGRATION MATRIX
31 M=K3-2
33 N=K3-1
34 A=K3
35 A=1./(3.*A)
37 DO 10 K=2,M,2
41 10 D(K)=2.*A
46 DO 15 K=1,N,2
47 15 D(K)=4.*A
54 D(K3)=A
* CALCULATE NONHOMOGENEOUS TERMS
56 RHS=1.0
57 DO 22 I=1,K2
61 PRINT 9
64 9 FORMAT(1H1)
64 READ 61,BMU
72 61 FORMAT(F10.5)
72 DO 999 II=1,K4
74 DO 35 N=1,K3
75 35 NON(N)=RHS*PT(N)
* CALCULATE KERNEL MATRICES
102 CALL CONST(I)
103 DO 20 N=1,K3
105 DO 20 M=1,K3
106 IF(M-N)25,30,30
111 25 F(M,N,I)=F(N,M,I)
120 GO TO 20
120 30 F(M,N,I)=FU(I,PT(M),PT(N))
131 20 CONTINUE
136 CALL CHANGE(F,G,D,I)
141 CALL LINEQ(G,B,C, K3)
144 DO 40 L=1,K3
146 PRINT 6,PT(L),NON(L)
155 6 FORMAT(5X,F8.4,F15.6)
155 40 CONTINUE
160 LP(II+1)=NON(K3)
162 DTA(II+1)=P
164 999 CONTINUE
166 PUNCH 66,(DTA(IX),LP(IX),IX=1,19)
202 66 FORMAT(2F10.5)
202 CALL LAPINV(DTA,LP)
204 22 CONTINUE
207 END

```

```

6 FUNCTION SIMP(I,A,B)
6 COMMON/AUX/H,P,PK1,PK2,BMU,X,Y
10 DEL=0.25*(B-A)
12 IF(DEL)40,45,50
13 SIMP=0.0
13 RETURN
14 50 CONTINUE
14 SA=Z(I,A)+Z(I,B)
26 SB=Z(I,A+2.*DEL)
35 SC=Z(I,A+DEL)+Z(I,A+3.*DEL)

```

```

53      S1=(DEL/3.)*(SA+2.*SB+4.*SC)
61      IF(S1.EQ.0.0) GO TO 45
62      K=8
63      35  S3=SB+SC
65      DEL=0.5*DEL
67      SC=Z(I,A+DEL)
75      J=K-1
77      DO 5 N=3,J,2
100     AN=N
101     5   SC=SC+Z(I,A+AN*DEL)
113     S2=(DEL/3.)*(SA+2.*SB+4.*SC)
122     DIF=ABS((S2-S1)/S1)
125     ER=0.01
127     IF(DIF-ER) 30,25,25
131     30  SIMP=S2
133     RETURN
134     25  K=2*K
136     S1=S2
140     IF(K-2048) 35,35,40
142     PRINT 42,I,A,E
152     42  FORMAT(5X,* INT. DOES NOT CONVERGE *,I3,2F9.4)
162     PRINT 60,X,Y
162     60  FORMAT(2F10.5)
166     DO 70 J=1,10
167     DIP=J
171     DIP=DIP/10.
175     W=Z(I,DIF)
202     PRINT 60,W
206     70  CONTINUE
207     CALL EXIT
      END

```

```

7      SUBROUTINE CHANGE(F,G,D,I)
7      REAL F(4,4,1),G(4,4),D(4)
7      COMMON K1,K2,K3,K4
10     DO 10 N=1,K3
11     DO 10 M=1,K3
24     10  G(M,N)=F(M,N,I)*D(N)
30     CONTINUE
31     20  DO 20 N=1,K3
40     20  G(N,N)=G(N,N)+1.0
41     RETURN
      END

```

```

7      SUBROUTINE LINEG(A,B,T,N)
7      REAL A(N,N),E(N),T(N)
10     DO 5 I=2,N
17     5   A(I,1)=A(I,1)/A(1,1)
20     DO 10 K=2,N
22     M=K-1
23     DO 15 I=1,N
33     15  T(I)=A(I,K)
34     DO 20 J=1,M
41     A(J,K)=T(J)
43     J1=J+1
44     DO 20 I=J1,N
55     20  T(I)=T(I)-A(I,J)*A(J,K)
61     CONTINUE
65     A(K,K)=T(K)
66     IF(K.EQ.N) GO TO 10
70     M=K+1
71     DO 25 I=M,N
105    25  A(I,K)=T(I)/A(K,K)
110    *   10  CONTINUE
111    *   BACK SUBSTITUTE
114    DO 30 I=1,N
116    T(I)=B(I)
121    M=I+1
122    IF(M.GT.N) GO TO 30
132    DO 30 J=M,N
136    30  B(J)=B(J)-A(J,I)*T(I)
      DO 35 I=1,N

```

```

37 K=N+1-I
41 B(K)=T(K)/A(K,K)
46 K1=K-1
50 IF(K1.EQ.0) GO TO 35
51 DO 35 J1=1,K1
52 J=K-J1
54 T(J)=T(J)-A(J,K)*B(K)
62 35 CONTINUE
67 RETURN
67 END

```

```

6 FUNCTION FU(I,A,B)
6 COMMON/AUX/H,P,PK1,PK2,BMU,X,Y
7 X=A
7 Y=B
10 IF(A*B)5,10,5
11 FU=0.0
12 RETURN
13 5 SUM=SIMP(I,0.0,5.0)
20 ER=0.01
21 DEL =5.0
23 20 UP=DEL+5.0
25 ADDL=SIMP(I,DEL,UP)
32 DEL =UP
33 TEST=ABS(ADDL/SUM)
36 SUM=SUM+ADDL
37 IF(TEST-ER)15,20,20
41 15 FU=SQRT(X*Y)*SUM
47 RETURN
47 END

```

```

3 SUBROUTINE CONST(I)
3 COMMON/AUX/H,P,PK1,PK2,BMU,X,Y
3 PR1=0.29
6 PR2=0.29
6 PK1=SQRT(((1.-2.*PR1)/(2.*(1.-PR1)))
15 PK2=SQRT(((1.-2.*PR2)/(2.*(1.-PR2)))
24 READ 1,P
31 1 FORMAT(F10.5)
31 HH=0.1
33 HH=10.0
34 HH=5.0
36 HH=4.0
37 HH=1.0
41 HH=0.5
42 HH=2.0
44 H=1./HH
45 PRINT 2,BMU,PR1,PR2,HH,P
62 2 FORMAT(////5X,* MU2/MU1 =*F6.2,* NU1 =*F4.2,* NU2 =*F4.2/5X,* A
62 1/H =*F4.2,* C21/PA =*F4.2)
63 RETURN
63 END

```

```

5 FUNCTION Z(I,S)
5 COMMON/AUX/H,P,PK1,PK2,BMU,X,Y
23 BESJH(A)=SQRT(2.*A/PI)*SIN(A)/A
25 PI=3.1415926
27 IF(S-0.0)5,5,10
30 5 Z=0.0
31 RETURN
31 10 CONTINUE
31 PP=P*P
33 C1=PK1*PK1
34 C2=PK2*PK2
36 CC=1.-C1
40 GA=SQRT(S*S+C1/PP)
46 GB=SQRT(S*S+1./PP)
55 GC=SQRT(S*S+C2/BMU/PP)
64 GD=SQRT(S*S+1./BMU/PP)
73 AA=S*S+1./PP/2.
77 AB=1.-BML

```

100
103
110
115
123
131
137
145
152
157
162
164
171
174
200
203
206
211
214
217
222
226
231
233
235
236
240
242
244
246
247
252
256
266
275
301
307
312
321
322
337
347
350

```

AC=S*S-GC*GD
AD=(GB-GD)/AC/PP/2.*BMU
AF=(GB+GD)/AC/PP/2.*BMU
AF=(S*S-GA*GD)/AC/PP/2.*EMU
AG=(S*S+GA*GD)/AC/PP/2.*EMU
AH=(S*S-GB*GC)/AC/PP/2.*BMU
AI=(S*S+GB*GC)/AC/PP/2.*BMU
AJ=(GA-GC)/AC/PP/2.*BMU
AK=(GA+GC)/AC/PP/2.*BMU
A1=- (AB*GB-AD)
A2=AB*GB-AE
A3=AA-BMU*S*S-AF
A4=AA-BMU*S*S-AG
A5=-AA+BMU*S*S-AH
A6=-AA+BMU*S*S-AI
A7=S*(AE*GA-AJ)
A8=-S*(AE*GA-AK)
BA=A1*A6-A2*A5
BB=A3*A6-S*A2*A7
BC=A4*A6-S*A2*A8
BD=S*A1*A7-A3*A5
BE=S*A1*A8-A4*A5
B1=BB/BA
B2=BC/BA
B3=BD/BA
B4=BE/BA
EA=2.*GA*H
EB=2.*GB*H
EC=(EA+EB)/2.
ED=2.*GC
E1=EXP(-EA)
E2=EXP(-EB)
E3=EXP(-EC)
E4=EXP(-ED)
DL=B2+B3*E4+B4*E2+B1*E1
D1=2.*PP/CC/GB/DL
D2=AA*AA-S*S*GA*GB
D3=B2-B3*E4
D4=2.*AA*(GB*(B1*B4-B2*B3)-S*S*GA)*E3
D5=(AA*AA+S*S*GA*GB)*(B4*E2-B1*E1)
F=D1*(D2*D3+D4+D5)
Z=(F-S)*EESJH(S*X)*BESJH(S*Y)
RETURN
END

```

C
C
C

100
103
110
115
123
131
137
145
152
157
162
164
171
174
200
203
206
211
214
217
222
226
231
233
235
236
240
242
244
246
247
252
256
266
275
301
307
312
321
322
337
347
350

```

SUBROUTINE LAPINV(GLAM,PHI)
THIS PROGRAM EVALUATES THE COEFFICIENTS FOR SERIES
OF JACOBI POLYNOMIALS WHICH REPRESENTS A LAPLACE
INVERSION INTEGRAL
REAL MUL
DIMENSION A(50),GLAM(50),PHI(50),C(4,50)
DIMENSION BK(101),TT(101)
COMMON/2/TT,TF,DT,MN,EK,TT
READ 1,NN,MN,MM
1 FORMAT(3I2)
READ 2,TT,TF,DT
2 FORMAT(3F10.5)
PRINT 99
99 FORMAT(1H1)
CALL SPLICE(GLAM,PHI,MM,C)
PRINT 101
101 FORMAT(/////5X,* GLAM PHI *)
PRINT 102,(GLAM(I),PHI(I),I=1,MM)
102 FORMAT(5X,F10.5,5X,F10.5)
M11=MM-1
PRINT 300
300 FORMAT(/////5X,* C(1,J) C(2,J) C(3,J) C(4,
1,J) *)
PRINT 103,((C(I,J),I=1,4),J=1,M11)
103 FORMAT(5X,F10.5,5X,F10.5,5X,F10.5,5X,F10.5)
PRINT 99
DO 10 I=1,NN
READ 3,BET,DEL
3 FORMAT(2F10.5)
PRINT 98,BET,DEL

```

```

140 98 FORMAT(/////5X,*BETA =*F5.3,* DELTA =*F5.3)
140 DO 11 L=1,MN
143 AL=L
144 S=1./(AL+BET)/DEL
150 CALL SPLINE(GLAM,PHI,MM,C,S,G)
153 F=G*S
155 IF(AL-2.)81,82,83
161 81 A(1)=(1.+BET)*DEL*F
165 GO TO 11
165 82 A(2)=((2.+BET)*DEL*F-A(1))*(3.+BET)
175 GO TO 11
175 83 CONTINUE
177 TOP=1.
177 L1=L-1
201 AL1=L1
202 DO 12 J=1,L1
203 AJ=J
204 TOP=AJ*TOP
206 12 CONTINUE
210 L2=2*L-1
212 BOT=1.
214 DO 13 J=L,L2
215 AJ=J
216 BOT=(AJ+BET)*BOT
221 13 CONTINUE
223 MUL=BOT/TOP
225 SUM=0.0
226 DO 14 N=1,L1
227 AN=N
230 IF(AN-2.)85,86,87
233 85 TOC=1.
235 GO TO 88
235 86 TOD=AL1
237 GO TO 88
237 87 CONTINUE
237 TOD=1.
241 ICH=L1-(N-2)
244 DO 15 J=ICH,L1
245 AJ=J
246 TOC=AJ*TOD
250 15 CONTINUE
252 88 CONTINUE
252 BOD=1.
254 JA=L1+N
256 DO 16 J=L,JA
256 AJ=J
261 BOD=BOD*(AJ+BET)
264 16 CONTINUE
266 CO=TOD/BOD
270 SUM=SUM+CO*A(N)
273 14 CONTINUE
275 A(L)=MUL*(DEL*F-SUM)
301 11 CONTINUE
304 CALL JACSER(DEL,A,BET)
306 CALL NAMPLT
307 CALL QIKSET(6.0,0.0,0.0,0.0,E.0,0.0,0.0)
313 CALL QIKSAX(3,3)
315 CALL QIKFLT(TT,BK,101)
320 CALL ENDFLT
321 10 CONTINUE
325 999 CONTINUE
325 RETURN
326 END

```

```

6 SUBROUTINE JACSER(D,C,B)
6 DIMENSION C(50),SF(50),P(50)
6 DIMENSION BK(101),TT(101)
6 COMMON/2/TT,TF,DT,MN,BK,TT
7 TT(1)=0.0
7 BK(1)=0.0
10 LM=1
11 T=TT
12 12 T=T+DT
14 X=2.*EXP(-D*T)-1.
24 CALL JACOBI(MN,X,B,P)

```

```

26 SF(1)=C(1)*P(1)
32 DO 10 L=2,MN
33 L1=L-1
35 AL=L
36 SF(L)=SF(L1)+C(L)*P(L)
43 10 CONTINUE
45 PRINT 97,T,X
55 97 FORMAT(///5X,* T =*F6.3,* X =*F10.5)
55 PRINT 96
61 96 FORMAT(///5X,* I C(I) *,5X,* N F(T) *)
61 DO 11 I=1,6
65 PRINT 95,I,C(I),I,SF(I)
105 95 FORMAT(5X,I2,F10.2,5X,I2,F10.5)
105 11 CONTINUE
111 LM=LM+1
113 BK(LM)=SF(5)
115 TT(LM)=T
117 IF(T.LE.TF) GO TO 12
121 RETURN
122 END

```

C SUBROUTINE JACOBI(N,X,B,FB)
THIS PROGRAM CALCULATES JACOBI POLYNOMIALS OF ORDER
K-1 WITH ARG X AND PARAMETER B GT -1

```

7 DIMENSION PB(N)
7 AN=N
10 IF (AN-2.) 1,2,3
12 1 PB(1)=1.
14 RETURN
14 2 PB(1)=1.
16 PB(2)=X-B*(1.-X)/2.
21 RETURN
22 3 BSQ=B*B
23 BONE=B+1.
25 PB(1)=1.
26 PB(2)=X-B*(1.-X)/2.
31 DO 4 K=3,N
33 AK=K
34 AK1=AK-1.
36 AK2=AK-2.
40 K1=K-1
42 K2=K-2
43 CO1=((2.*AK1)+B)*X
46 CO1=((2.*AK2)+B)*CO1
48 CO1=((2.*AK2)+BONE)*(CO1-BSQ)
51 CO2=2.*AK2*(AK2+B)*((2.*AK1)+B)
56 CO2=2.*AK1*(AK1+B)*((2.*AK2)+B)
64 4 PB(K)=(CO1*PB(K1)-CO2*PB(K2))/CO
71 RETURN
102 END
103

```

```

11 SUBROUTINE SPLINE(X,Y,M,C,XINT,YINT)
11 DIMENSION X(50),Y(50),C(4,50)
13 IF (XINT-X(1)) 1,10,11
14 10 YINT=Y(1)
14 RETURN
15 11 CONTINUE
15 IF (X(M)-XINT) 1,12,13
21 12 YINT=Y(M)
23 RETURN
23 13 CONTINUE
23 K=M/2
25 N=M
26 2 CONTINUE
26 IF (X(K)-XINT) 3,14,5
32 14 YINT=Y(K)
34 RETURN
35 3 CONTINUE
35 IF (XINT-X(K+1)) 4,15,7
41 15 YINT=Y(K+1)
43 RETURN
43 4 CONTINUE
43 YINT=(X(K+1)-XINT)*(C(1,K)+(X(K+1)-XINT)**2+C(3,K))

```

```

54      YINT=YINT+(XINT-X(K))*(C(2,K)*(XINT-X(K))**2+C(4,K))
65      RETURN
65      5 CONTINUE
65      IF(X(K-1)-XINT)6,16,17
70      6 K=K-1
72      GO TO 4
72      16 YINT=Y(K-1)
74      RETURN
75      17 N=K
77      K=K/2
100     GO TO 2
100     7 LL=K
102     K=(N+K)/2
103     8 CONTINUE
103     IF(X(K)-XINT)3,14,18
106     18 CONTINUE
106     IF(X(K-1)-XINT)6,16,19
111     19 N=K
113     K=(LL+K)/2
114     GO TO 8
115     1 PRINT 101
121     101 FORMAT(* OUT OF RANGE FOR INTERPOLATION *)
121     STOP
123     END

```

```

7      SUBROUTINE SPLICE(X,Y,M,C)
7      DIMENSION X(50),Y(50),D(50),P(50),E(50),C(4,50)
7      DIMENSION A(50,3),B(50),Z(50)
11     MM=M-1
12     DO 2 K=1,MM
15     D(K)=X(K+1)-X(K)
15     P(K)=D(K)/6.
20     2 E(K)=(Y(K+1)-Y(K))/D(K)
26     DO 3 K=2,MM
27     3 B(K)=E(K)-E(K-1)
34     A(1,2)=-1.-D(1)/D(2)
37     A(1,3)=D(1)/D(2)
41     A(2,3)=P(2)-P(1)*A(1,3)
44     A(2,2)=2.*(P(1)+P(2))-P(1)*A(1,2)
50     A(2,3)=A(2,3)/A(2,2)
51     B(2)=B(2)/A(2,2)
53     DO 4 K=3,MM
54     A(K,2)=2.*(P(K-1)+P(K))-P(K-1)*A(K-1,3)
61     B(K)=B(K)-P(K-1)*B(K-1)
65     A(K,3)=P(K)/A(K,2)
70     4 B(K)=B(K)/A(K,2)
74     Q=D(M-2)/D(M-1)
76     A(M,1)=1.+Q+A(M-2,3)
101    A(M,2)=-Q-A(M,1)*A(M-1,3)
105    B(M)=B(M-2)-A(M,1)*B(M-1)
112    Z(M)=B(M)/A(M,2)
114    MN=M-2
116    DO 6 I=1,MN
117    K=M-I
120    6 Z(K)=B(K)-A(K,3)*Z(K+1)
127    Z(1)=-A(1,2)*Z(2)-A(1,3)*Z(3)
133    DO 7 K=1,MM
135    Q=1./(6.*D(K))
140    C(1,K)=Z(K)*Q
143    C(2,K)=Z(K+1)*Q
146    C(3,K)=Y(K)/D(K)-Z(K)*P(K)
154    7 C(4,K)=Y(K+1)/D(K)-Z(K+1)*P(K)
165    RETURN
165    END

```

Torsional impact

```

3      PROGRAM BETA(INPUT,OUTPUT,PUNCH,PLOT,TAPE 99=PLOT)
3      REAL NON(4),F(4,4,1),G(4,4),D(4),PT(4)
3      REAL B(4),C(4)
3      REAL LP(50),DTA(50)
3      EQUIVALENCE (NON,B)
3      COMMON K1,K2,K3,K4
3      COMMON/AUX/H,P,PK1,PK2,BMU,X,Y
4      LP(1)=0.0
4      DTA(1)=0.0
5      READ 2,K1,K2,K3,K4
20     FORMAT(I2)
*      2  = ORDER OF SYSTEM OF EQUATIONS
*      K2 = NO. OF DISTINCT KERNELS
*      K3 = NO. OF DATA POINTS
*      K4 = NO. OF DATA SETS TO BE EVALUATED
*      SET UP DATA POINTS
20     AK=K3
22     DO 5 N=1,K3
23     AN=N
24     5  PT(N)=AN/AK
*      SET UP INTEGRATION MATRIX
31     M=K3-2
33     N=K3-1
34     A=K3
35     A=1./(3.*A)
37     DO 10 K=2,M,2
41     10 D(K)=2.*A
46     DO 15 K=1,N,2
47     15 D(K)=4.*A
54     D(K3)=A
*      CALCULATE NONHOMOGENEOUS TERMS
56     RHS=1.0
57     DO 22 I=1,K2
61     PRINT 9
64     9  FORMAT(1H1)
64     READ 61,BMU
72     61 FORMAT(F10.5)
72     DO 999 II=1,K4
74     DC 35 N=1,K3
75     35 NON(N)=RHS*PT(N)*PT(N)
*      CALCULATE KERNEL MATRICES
102    CALL CONST(I)
104    DO 20 N=1,K3
106    DO 20 M=1,K3
107    IF(M-N)25,30,30
112    25 F(M,N,I)=F(N,M,I)
121    GC TO 20
121    30 F(M,N,I)=FU(I,PT(M),PT(N))
132    20 CONTINUE
137    CALL CHANGE(F,G,D,I)
142    CALL LINEQ(G,B,C, K3)
145    DO 40 L=1,K3
147    PRINT 6,PT(L),NON(L)
156    6  FORMAT(5X,F8.4,F15.6)
156    40 CONTINUE
161    LP(II+1)=NON(K3)
163    DTA(II+1)=P
165    999 CONTINUE
167    PUNCH 66,(DTA(IX),LP(IX),IX=1,19)
203    66 FORMAT(2F10.5)
203    CALL LAPINV(DTA,LP)
205    22 CONTINUE
210    END

```

```

6      FUNCTION SIMP(I,A,B)
6      COMMON/AUX/H,P,PK1,PK2,BMU,X,Y
10     DEL=0.25*(B-A)
12     IF(DEL)40,45,50
13     SIMP=0.0
13     RETURN
14     50 CONTINUE
14     SA=Z(I,A)+Z(I,B)
16     SB=Z(I,A+2.*DEL)
15     SC=Z(I,A+DEL)+Z(I,A+3.*DEL)

```

```

53      S1=(DEL/3.)*(SA+2.*SB+4.*SC)
61      IF(S1.EQ.0.0) GO TO 45
62      K=8
63      35  SB=SB+SC
65      DEL=0.5*DEL
67      SC=Z(I,A+DEL)
75      J=K-1
77      DO 5 N=3,J,2
100     AN=N
101     5   S(=SC+Z(I,A+AN*DEL)
113     S2=(DEL/3.)*(SA+2.*SB+4.*SC)
122     DIF=ABS((S2-S1)/S1)
125     ER=0.01
127     IF(DIF-ER)30,25,25
131     30  SIMP=S2
133     RETURN
134     25  K=2*K
136     S1=S2
140     IF(K-2048)35,35,40
152     40  PRINT 42,I,A,B
152     42  FORMAT(5X,* INT. DOES NOT CONVERGE *,I3,2F9.4)
162     PRINT 60,X,Y
162     60  FORMAT(2F10.5)
166     DO 70 J=1,10
167     DIP=J
171     DIP=DIP/10.
175     W=Z(I,DIP)
202     PRINT 60,W
206     70  CONTINUE
207     CALL EXIT
      END

```

```

7      SUBROUTINE CHANGE(F,G,D,I)
7      REAL F(4,4,1),G(4,4),D(4)
7      COMMON K1,K2,K3,K4
10     DO 10 N=1,K3
11     DC 10 M=1,K3
24     10  G(M,N)=F(M,N,I)*D(N)
30     CONTINUE
31     20  DO 20 N=1,K3
40     G(N,N)=G(N,N)+1.0
41     RETURN
      END

```

```

7      SUBROUTINE LINEQ(A,B,T,N)
7      REAL A(N,N),B(N),T(N)
17     5   DO 5 I=2,N
20     A(I,1)=A(I,1)/A(1,1)
22     DO 10 K=2,N
23     M=K-1
33     15  DO 15 I=1,N
34     T(I)=A(I,K)
41     DC 20 J=1,M
43     A(J,K)=T(J)
44     J1=J+1
44     DC 20 I=J1,N
55     20  T(I)=T(I)-A(I,J)*A(J,K)
61     CONTINUE
65     A(K,K)=T(K)
66     IF(K.EQ.N) GO TO 10
70     M=K+1
71     DO 25 I=M,N
105    25  A(I,K)=T(I)/A(K,K)
110    10  CONTINUE
111    *  BACK SUBSTITUTE
114    DO 30 I=1,N
116    T(I)=B(I)
121    M=I+1
122    IF(M.GT.N) GO TO 30
126    DO 30 J=M,N
136    B(J)=B(J)-A(J,I)*T(I)
141    30  CONTINUE
146    DO 35 I=1,N

```



```

SUBROUTINE LAPINV (GLAM,PHI)
THIS PROGRAM EVALUATES THE COEFFICIENTS FOR SERIES
OF JACOBI POLYNOMIALS WHICH REPRESENTS A LAPLACE
INVERSION INTEGRAL
REAL MUL
DIMENSION A(50),GLAM(50),PHI(50),C(4,50)
DIMENSION BK(101),TT(101)
COMMON/2/TI,TF,DT,MN,BK,TT
READ 1,NN,MN,MM
1 FORMAT(3I2)
READ 2,TI,TF,DT
2 FORMAT(3F10.5)
PRINT 99
99 FORMAT(1H1)
CALL SPLICE (GLAM,PHI,MM,C)
PRINT 101
101 FORMAT(/////5X,*      GLAM          PHI      *)
PRINT 102,(GLAM(I),PHI(I),I=1,MM)
102 FORMAT(5X,F10.5,5X,F10.5)
M11=MM-1
PRINT 300
300 FORMAT(/////5X,*      C(1,J)          C(2,J)          C(3,J)          C(4
1,J) *)
PRINT 103,((C(I,J),I=1,4),J=1,M11)
103 FORMAT(5X,F10.5,5X,F10.5,5X,F10.5,5X,F10.5)
PRINT 99
DO 10 I=1,NN
READ 3,BET,DEL
3 FORMAT(2F10.5)
PRINT 98,BET,DEL
98 FORMAT(/////5X,*BETA =*F5.3,* DELTA =*F5.3)
DO 11 L=1,MN
AL=L
S=1./(AL+BET)/DEL
CALL SPLINE (GLAM,PHI,MM,C,S,G)
F=G*S
IF (AL-2.) 81,82,83
81 A(1)=(1.+BET)*DEL*F
GO TO 11
82 A(2)=((2.+BET)*DEL*F-A(1))*(3.+BET)
GO TO 11
83 CONTINUE
TOP=1.
L1=L-1
AL1=L1
DO 12 J=1,L1
AJ=J
TOP=AJ*TOP
12 CONTINUE
L2=2*L-1
BOT=1.
DO 13 J=L,L2
AJ=J
BOT=(AJ+BET)*BOT
13 CONTINUE
MUL=BOT/TOP
SUM=0.0
DO 14 N=1,L1
AN=N
IF (AN-2.) 85,86,87
85 TOD=1.
GO TO 88
86 TOD=AL1
GO TO 88
87 CONTINUE
TOD=1.
ICH=L1-(N-2)
DO 15 J=ICH,L1
AJ=J
TOD=AJ*TOD
15 CONTINUE
88 CONTINUE
BOO=1.
JA=L1+N
DO 16 J=L,JA
AJ=J

```

```

2 61      BOD=BOD*(AJ+BET)
2 64      16 CONTINUE
2 66      CO=TOD/BOD
2 70      SUM=SUM+CO*A(N)
2 73      14 CONTINUE
2 75      A(L)=MUL*(DEL*F-SUM)
3 01      11 CONTINUE
3 04      CALL JACSER(DEL,A,BET)
3 06      CALL NAMPLT
3 07      CALL QIKSET(6.0,0.0,0.0,6.0,0.0,0.0)
3 13      CALL QIKSAX(3,3)
3 15      CALL QIKPLT(TT,BK,101)
3 20      CALL ENDPLT
3 21      10 CONTINUE
3 25      999 CONTINUE
3 25      RETURN
3 26      END

```

```

6          SUBROUTINE JACSER(D,C,B)
6          DIMENSION C(50),SF(50),P(50)
6          DIMENSION BK(101),TT(101)
6          COMMON/2/TT,TF,DT,MN,BK,TT
7          TT(1)=0.0
7          BK(1)=0.0
10         LM=1
11         T=TI
12         12 T=T+DT
14         X=2.*EXP(-D*T)-1.
24         CALL JACOBI(MN,X,B,P)
26         SF(1)=C(1)*P(1)
32         DO 10 L=2,MN
33         L1=L-1
35         AL=L
36         SF(L)=SF(L1)+C(L)*P(L)
43         10 CONTINUE
45         PRINT 97,T,X
55         97 FORMAT(///5X,* T=*F6.3,* X=*F10.5)
55         PRINT 96
61         96 FORMAT(///5X,* I C(I) *,5X,* N F(T) *)
61         DO 11 I=1,6
65         PRINT 95,I,C(I),I,SF(I)
1 05        95 FORMAT(5X,I2,F10.2,5X,I2,F10.5)
1 05        11 CONTINUE
1 11        LM=LM+1
1 13        BK(LM)=SF(5)
1 15        TT(LM)=T
1 17        IF(T.LE.TF) GO TO 12
1 21        RETURN
1 22        END

```

```

C          SUBROUTINE JACOBI(N,X,B,PB)
C          THIS PROGRAM CALCULATES JACOBI POLYNOMIALS OF ORDER
C          K-1 WITH ARG X AND PARAMETER B GT -1
7          DIMENSION PB(N)
7          A=N
7          IF(A.NE.2.) 1,2,3
10         1 PB(1)=1.
12         RETURN
14         2 PB(1)=1.
14         PB(2)=X-B*(1.-X)/2.
16         RETURN
16         3 BSQ=B*B
21         BONE=B+1.
22         PB(1)=1.
23         PB(2)=X-B*(1.-X)/2.
25         DO 4 K=3,N
26         AK=K
27         AK1=AK-1.
28         AK2=AK-2.
31         K1=K-1
32         K2=K-2
33         CO1=((2.*AK1)+B)*X
34         CO1=((2.*AK2)+B)*CO1
36
37
38
39
40
41
42
43
44
45
46

```

```

51      CO1=((2.*AK2)+BONE)*(CO1-BSQ)
56      CO2=2.*AK2*(AK2+B)*((2.*AK1)+B)
64      CO=2.*AK1*(AK1+B)*((2.*AK2)+B)
71      4 PB(K)=(CO1*PB(K1)-CO2*PB(K2))/CO
1 02      RETURN
1 03      END

```

```

11      SUBROUTINE SPLINE (X,Y,M,C,XINT,YINT)
11      DIMENSION X(50),Y(50),C(4,50)
13      IF(XINT-X(1))1,10,11
14      10 YINT=Y(1)
14      RETURN
15      11 CONTINUE
15      IF(X(M)-XINT)1,12,13
16      12 YINT=Y(M)
16      RETURN
17      13 CONTINUE
17      K=M/2
17      N=M
18      2 CONTINUE
18      IF(X(K)-XINT)3,14,5
19      14 YINT=Y(K)
19      RETURN
20      3 CONTINUE
20      IF(XINT-X(K+1))4,15,7
21      15 YINT=Y(K+1)
21      RETURN
22      4 CONTINUE
22      YINT=(X(K+1)-XINT)*(C(1,K)*(X(K+1)-XINT)**2+C(3,K))
23      YINT=YINT+(XINT-X(K))*(C(2,K)*(XINT-X(K))**2+C(4,K))
24      RETURN
25      5 CONTINUE
25      IF(X(K-1)-XINT)6,16,17
26      6 K=K-1
26      GO TO 4
27      16 YINT=Y(K-1)
27      RETURN
28      17 N=K
28      K=K/2
28      GO TO 2
29      7 LL=K
29      K=(N+K)/2
30      8 CONTINUE
30      IF(X(K)-XINT)3,14,13
31      18 CONTINUE
31      IF(X(K-1)-XINT)6,16,19
32      19 N=K
32      K=(LL+K)/2
32      GO TO 8
33      1 PRINT 101
34      101 FORMAT(* OUT OF RANGE FOR INTERPOLATION *)
35      STOP
36      END

```

```

7      SUBROUTINE SPLICE (X,Y,M,C)
7      DIMENSION X(50),Y(50),D(50),P(50),E(50),C(4,50)
7      DIMENSION A(50,3),B(50),Z(50)
8      MM=M-1
9      DO 2 K=1,MM
10     D(K)=X(K+1)-X(K)
11     P(K)=D(K)/6.
12     2 E(K)=(Y(K+1)-Y(K))/D(K)
13     DO 3 K=2,MM
14     B(K)=E(K)-E(K-1)
15     A(1,2)=-1.-D(1)/D(2)
16     A(1,3)=D(1)/D(2)
17     A(2,3)=P(2)-P(1)*A(1,3)
18     A(2,2)=2.*(P(1)+P(2))-P(1)*A(1,2)
19     A(2,3)=A(2,3)/A(2,2)
20     B(2)=B(2)/A(2,2)
21     DO 4 K=3,MM
22     A(K,2)=2.*(P(K-1)+P(K))-P(K-1)*A(K-1,3)
23     B(K)=B(K)-P(K-1)*B(K-1)

```

```

65      A(K,3)=P(K)/A(K,2)
70      4 B(K)=B(K)/A(K,2)
74      Q=D(M-2)/D(M-1)
76      A(M,1)=1.+Q+A(M-2,3)
101     A(M,2)=-Q-A(M,1)*A(M-1,3)
105     B(M)=B(M-2)-A(M,1)*B(M-1)
112     Z(M)=B(M)/A(M,2)
114     MN=M-2
116     DO 6 I=1,MN
117     K=M-I
120     6 Z(K)=B(K)-A(K,3)*Z(K+1)
127     Z(1)=-A(1,2)*Z(2)-A(1,3)*Z(3)
133     DO 7 K=1,MM
135     Q=1./(6.*D(K))
140     C(1,K)=Z(K)*Q
143     C(2,K)=Z(K+1)*Q
146     C(3,K)=Y(K)/D(K)-Z(K)*P(K)
154     7 C(4,K)=Y(K+1)/D(K)-Z(K+1)*P(K)
165     RETURN
165     END

```

INTERIM REPORT DISTRIBUTION LIST

NSG 3179

"NORMAL AND RADIAL IMPACT OF COMPOSITES WITH EMBEDDED
PENNY-SHAPED CRACKS"

Advanced Research Projects Agency
Washington DC 20525
Attn: Library

Advanced Technology Center, Inc.
LTV Aerospace Corporation
P.O. Box 6144
Dallas, TX 75222
Attn: D. H. Petersen
W. J. Renton

Air Force Flight Dynamics Laboratory
Wright-Patterson Air Force Base, OH 45433
Attn: L. J. Obery (TBP)
G. P. Sendeckyj (FBC)
R. S. Sandhu

Air Force Materials Laboratory
Wright-Patterson Air Force Base, OH 45433
Attn: H. S. Schwartz (LN)
T. J. Reinhart (MBC)
G. P. Peterson (LC)
E. J. Morrisey (LAE)
S. W. Tsai (MBM)
N. J. Pagano
J. M. Whitney (MBM)

Air Force Office of Scientific Research
Washington DC 20333
Attn: J. F. Masi (SREP)

Air Force Office of Scientific Research
1400 Wilson Blvd.
Arlington, VA 22209

AFOSR/NA
Bolling AFB, DC 20332
Attn: W. J. Walker

Air Force Rocket Propulsion Laboratory
Edwards, CA 93523
Attn: Library

Babcock & Wilcox Company
Advanced Composites Department
P.O. Box 419
Alliance, Ohio 44601
Attn: P. M. Leopold

Bell Helicopter Company
P.O. Box 482
Ft. Worth, TX 76101
Attn: H. Zinberg

The Boeing Company
P. O. Box 3999
Seattle, WA 98124
Attn: J. T. Hoggatt, MS. 88-33
T. R. Porter

The Boeing Company
Vertol Division
Morton, PA 19070
Attn: R. A. Pinckney
E. C. Durchlaub

Battelle Memorial Institute
Columbus Laboratories
505 King Avenue
Columbus, OH 43201
Attn: E. F. Rybicki
L. E. Hulbert

Brunswick Corporation
Defense Products Division
P. O. Box 4594
43000 Industrial Avenue
Lincoln, NE 68504
Attn: R. Morse

Celanese Research Company
86 Morris Ave.
Summit, NJ 07901
Attn: H. S. Kliger

Chemical Propulsion Information Agency
Applied Physics Laboratory
8621 Georgia Avenue
Silver Spring, MD 20910
Attn: Library

Commander
Natick Laboratories
U. S. Army
Natick, MA 01762
Attn: Library

Commander
Naval Air Systems Command
U. S. Navy Department
Washington DC 20360
Attn: M. Stander, AIR-43032D

Commander
Naval Ordnance Systems Command
U.S. Navy Department
Washington DC 20360
Attn: B. Drimmer, ORD-033
M. Kinna, ORD-033A

Cornell University
Dept. Theoretical & Applied Mech.
Thurston Hall
Ithaca, NY 14853
Attn: S. L. Phoenix

Defense Metals Information Center
Battelle Memorial Institute
Columbus Laboratories
505 King Avenue
Columbus, OH 43201

Department of the Army
U.S. Army Material Command
Washington DC 20315
Attn: AMCRD-RC

Department of the Army
U.S. Army Aviation Materials Laboratory
Ft. Eustis, VA 23604
Attn: I. E. Figge, Sr.
Library

Department of the Army
U.S. Army Aviation Systems Command
P.O. Box 209
St. Louis, MO 63166
Attn: R. Vollmer, AMSAV-A-UE

Department of the Army
Plastics Technical Evaluation Center
Picatinny Arsenal
Dover, NJ 07801
Attn: H. E. Pebly, Jr.

Department of the Army
Watervliet Arsenal
Watervliet, NY 12189
Attn: G. D'Andrea

Department of the Army
Watertown Arsenal
Watertown, MA 02172
Attn: A. Thomas

Department of the Army
Redstone Arsenal
Huntsville, AL 35809
Attn: R. J. Thompson, AMSMI-RSS

Department of the Navy
Naval Ordnance Laboratory
White Oak
Silver Spring, MD 20910
Attn: R. Simon

Department of the Navy
U.S. Naval Ship R&D Laboratory
Annapolis, MD 21402
Attn: C. Hersner, Code 2724

Director
Deep Submergence Systems Project
6900 Wisconsin Avenue
Washington DC 20015
Attn: H. Bernstein, DSSP-221

Director
Naval Research Laboratory
Washington DC 20390
Attn: Code 8430
I. Wolock, Code 8433

Drexel University
32nd and Chestnut Streets
Philadelphia, PA 19104
Attn: P. C. Chou

E. I. DuPont DeNemours & Co.
DuPont Experimental Station
Wilmington, DE 19898
Attn: C. H. Zweben

Fiber Science, Inc.
245 East 157 Street
Gardena, CA 90248
Attn: E. Dunahoo

General Dynamics
P.O. Box 748
Ft. Worth, TX 76100
Attn: M. E. Waddoups
Library

General Dynamics/Convair
P.O. Box 1128
San Diego, CA 92112
Attn: J. L. Christian

General Electric Co.
Evendale, OH 45215
Attn: C. Stotler
R. Ravenhall
R. Stabrylla

General Motors Corporation
Detroit Diesel-Allison Division
Indianapolis, IN 46244
Attn: M. Herman

Georgia Institute of Technology
School of Aerospace Engineering
Atlanta, GA 30332
Attn: L. W. Rehfield

Grumman Aerospace Corporation
Bethpage, Long Island, NY 11714
Attn: S. Dastin
J. B. Whiteside

Hamilton Standard Division
United Aircraft Corporation
Windsor Locks, CT 06096
Attn: W. A. Percival

Hercules, Inc.
Allegheny Ballistics Laboratory
P. O. Box 210
Cumberland, MD 21053
Attn: A. A. Vicario

Hughes Aircraft Company
Culver City, CA 90230
Attn: A. Knoell

Illinois Institute of Technology
10 West 32 Street
Chicago, IL 60616
Attn: L. J. Broutman

IIT Research Institute
10 West 35 Street
Chicago, IL 60616
Attn: I. M. Daniel

Jet Propulsion Laboratory
4800 Oak Grove Drive
Pasadena, CA 91103
Attn: Library

Lawrence Livermore Laboratory
P.O. Box 808, L-421
Livermore, CA 94550
Attn: T. T. Chiao
E. M. Wu

Lehigh University
Institute of Fracture &
Solid Mechanics
Bethlehem, PA 18015
Attn: G. C. Sih

Lockheed-Georgia Co.
Advanced Composites Information Center
Dept. 72-14, Zone 402
Marietta, GA 30060
Attn: T. M. Hsu

Lockheed Missiles and Space Co.
P.O. Box 504
Sunnyvale, CA 94087
Attn: R. W. Fenn

Lockheed-California
Burbank, CA 91503
Attn: J. T. Ryder
K. N. Lauraitis
J. C. Ekvall

McDonnell Douglas Aircraft Corporation
P.O. Box 516
Lambert Field, MS 63166
Attn: J. C. Watson

McDonnell Douglas Aircraft Corporation
3855 Lakewood Blvd.
Long Beach, CA 90810
Attn: L. B. Greszczuk

Material Sciences Corporation
1777 Walton Road
Blue Bell, PA 19422
Attn: B. W. Rosen

Massachusetts Institute of Technology
Cambridge, MA 02139
Attn: F. J. McGarry
J. F. Mandell
J. W. Mar

NASA-Ames Research Center
Moffett Field, CA 94035
Attn: Library

NASA-Flight Research Center
P.O. Box 273
Edwards, CA 93523
Attn: Library

NASA-George C. Marshall Space Flight Center
Huntsville, AL 35812
Attn: C. E. Cataldo, S&E-ASTN-MX
Library

NASA-Goddard Space Flight Center
Greenbelt, MD 20771
Attn: Library

NASA-Langley Research Center
Hampton, VA 23365
Attn: E. E. Mathauser, MS 188a
R. A. Pride, MS 188a
M. C. Card
J. R. Davidson

NASA-Lewis Research Center
21000 Brookpark Road
Cleveland, Ohio 44135
Attn: Administration & Technical Service Section
Tech. Report Control, MS. 5-5
Tech. Utilization, MS 3-19
AFSC Liaison, MS. 501-3
Rel. and Quality Assur., MS 500-211
C. P. Blankenship, MS 105-1
R. F. Lark, MS 49-3
J. C. Freche, MS 49-1
R. H. Johns, MS 49-3
C. C. Chamis, MS 49-3 (17 copies)
T. T. Serafini, MS 49-1
Library, MS 60-3 (2 copies)

NASA-Lyndon B. Johnson Space Center
Houston, TX 77001
Attn: S. Glorioso, SMD-ES52
Library

NASA Scientific and Tech. Information Facility
P.O. Box 8757
Balt/Wash International Airport, MD 21240
Attn: Acquisitions Branch (10 copies)

National Aeronautics & Space Administration
Office of Advanced Research & Technology
Washington DC 20546
Attn: M. J. Salkind, Code RWS
D. P. Williams, Code RWS

National Aeronautics & Space Administration
Office of Technology Utilization
Washington DC 20546

National Bureau of Standards
Eng. Mech. Section
Washington DC 20234
Attn: R. Mitchell

National Technology Information Service
Springfield, VA 22151 (6 copies)

National Science Foundation
Engineering Division
1800 G. Street, NW
Washington DC 20540
Attn: Library

Northrop Corporation Aircraft Group
3901 West Broadway
Hawthorne, CA 90250
Attn: R. M. Verette
G. C. Grimes

Pratt & Whitney Aircraft
East Hartford, CT 06108
Attn: A. J. Dennis

Rockwell International
Los Angeles Division
International Airport
Los Angeles, CA 90009
Attn: L. M. Lackman
D. Y. Konishi

Sikorsky Aircraft Division
United Aircraft Corporation
Stratford, CT 06602
Attn: Library

Southern Methodist University
Dallas, TX 75275
Attn: R. M. Jones

Southwest Research Institute
8500 Culebra Road
San Antonio, TX 78284
Attn: P. H. Francis

Space & Missile Systems Organization
Air Force Unit Post Office
Los Angeles, CA 90045
Attn: Technical Data Center

Structural Composites Industries, Inc.
6344 N. Irwindale Avenue
Azusa, CA 91702
Attn: R. Gordon

Texas A&M
Mechanics & Materials Research Center
College Station, TX 77843
Attn: R. A. Schapery

TRW, Inc.
23555 Euclid Avenue
Cleveland, OH 44117
Attn: W. E. Winters

Union Carbide Corporation
P. O. Box 6116
Cleveland, OH 44101
Attn: J. C. Bowman

United Technologies Research Center
East Hartford, CT 06108
Attn: R. C. Novak

University of Dayton Research Institute
Dayton, OH 45409
Attn: R. W. Kim

University of Delaware
Mechanical & Aerospace Engineering
Newark, DE 19711
Attn: B. R. Pipes

University of Illinois
Department of Theoretical & Applied Mechanics
Urbana, IL 61801
Attn: S. S. Wang

University of Oklahoma
School of Aerospace Mechanical & Nuclear Engineering
Norman, OK 73069
Attn: C. W. Bert

University of Wyoming
College of Engineering
University Station Box 3295
Laramie, WY 82071
Attn: D. F. Adams

U. S. Army Materials & Mechanics Research Center
Watertown Arsenal
Watertown, MA 02172
Attn: E. M. Leno
D. W. Oplinger

V.P. I. and S. U.
Dept. of Eng. Mech.
Blacksburg, VA 24061
Attn: R. H. Heller
H. J. Brinson
C. T. Herakovich